

Assessing the Spurious Impacts of Ice-Constraining Methods on the Climate Response to Sea Ice Loss Using an Idealized Aquaplanet GCM

NEIL T. LEWIS^a, MARK R. ENGLAND,^a JAMES A. SCREEN,^a RUTH GEEN,^b REGAN MUDHAR,^a
WILLIAM J. M. SEVIOUR,^a AND STEPHEN I. THOMSON^a

^a *Department of Mathematics and Statistics, University of Exeter, Exeter, United Kingdom*

^b *School of Geography, Earth and Environmental Sciences, University of Birmingham, Birmingham, United Kingdom*

(Manuscript received 11 March 2024, in final form 13 August 2024, accepted 4 September 2024)

ABSTRACT: Coupled climate model simulations designed to isolate the effects of Arctic sea ice loss often apply artificial heating, either directly to the ice or through modification of the surface albedo, to constrain sea ice in the absence of other forcings. Recent work has shown that this approach may lead to an overestimation of the climate response to sea ice loss. In this study, we assess the spurious impacts of ice-constraining methods on the climate of an idealized aquaplanet general circulation model (GCM) with thermodynamic sea ice. The true effect of sea ice loss in this model is isolated by inducing ice loss through reduction of the freezing point of water, which does not require additional energy input. We compare the results of freezing point modification experiments with experiments where sea ice loss is induced using traditional ice-constraining methods and confirm the result of previous work that traditional methods induce spurious additional warming. Furthermore, additional warming leads to an overestimation of the circulation response to sea ice loss, which involves a weakening of the zonal wind and storm-track activity in midlatitudes. Our results suggest that coupled model simulations with constrained sea ice should be treated with caution, especially in boreal summer, where the true effect of sea ice loss is weakest, but we find the largest spurious response. Given that our results may be sensitive to the simplicity of the model we use, we suggest that devising methods to quantify the spurious effects of ice-constraining methods in more sophisticated models should be an urgent priority for future work.

SIGNIFICANCE STATEMENT: The potential effects of Arctic sea ice loss on midlatitude weather have been investigated using climate models where sea ice loss is artificially induced, without increasing greenhouse gas concentrations. Recently, this approach has been challenged because the artificial heating used to melt sea ice may also have direct effects on climate, which are not caused by sea ice loss. We run simulations with a simplified climate model that allows us to separate the “spurious” direct effects of the artificial heating from the “true” effect of sea ice loss. In our simulations, the responses of temperature and atmospheric circulation are amplified by spurious effects. Consequently, we argue that previous studies using more complex climate models may overestimate the effect of sea ice loss on climate.

KEYWORDS: Sea ice; Atmospheric circulation; Climate change; Idealized models


1. Introduction

The Arctic is undergoing rapid climate change, characterized by substantial sea ice loss and polar-amplified warming (Notz and Stroeve 2016; Screen and Simmonds 2010b), which has motivated study of the impacts of sea ice loss on weather and climate (Barnes and Screen 2015; Cohen et al. 2014, 2020).

To tackle this problem, numerous studies have made use of climate model simulations where sea ice loss is imposed. One approach has been to use atmospheric general circulation models (AGCMs), by comparing simulations where climatological or future sea ice concentrations (SICs) are prescribed while sea surface temperature (SST) is held fixed (see Barnes and Screen 2015 for a review). When sea ice loss occurs, some studies prescribe a fixed “freezing point” SST (e.g., Deser et al. 2010), while others prescribe SSTs from simulations of

future climate change, to account for sea surface warming associated with sea ice loss (e.g., Screen et al. 2013). Blackport and Kushner (2018) show that the response to sea ice loss is essentially insensitive to the chosen ice-free SST (see their Fig. 4b). AGCM experiments reveal that while Arctic sea ice loss is greatest in summer and autumn, the circulation response is greatest in winter (Deser et al. 2010). They consistently find that Arctic sea ice loss induces a weakening of the midlatitude westerlies [see Smith et al. 2022, which presents results from the Polar Amplification Model Intercomparison Project (PAMIP); Smith et al. 2019] but disagree on other aspects of change caused by sea ice loss, for example, the response of the stratosphere (Screen et al. 2018; Smith et al. 2022).

More recently, research into the impact of sea ice loss on climate has expanded to make use of coupled atmosphere-ocean GCMs (AOGCMs), which explicitly simulate interactions between the atmosphere, ocean, sea ice, and land (e.g., Deser et al. 2015; Blackport and Kushner 2016; Smith et al. 2017; McCusker et al. 2017; Smith et al. 2019; Sun et al. 2020). These studies investigate the response of AOGCMs to perturbed sea ice, by constraining sea ice area or volume, or

 Denotes content that is immediately available upon publication as open access.

Corresponding author: Neil T. Lewis, n.t.lewis@exeter.ac.uk

DOI: 10.1175/JCLI-D-24-0153.1

© 2024 American Meteorological Society. This published article is licensed under the terms of a Creative Commons Attribution 4.0 International (CC BY 4.0) License



both, to match that obtained in simulations of future climate change (using a variety of methods, discussed below), while keeping other climate forcings constant. Comparing AGCM and AOGCM experiments, Deser et al. (2015) find that including ocean coupling results in a warming response that extends to lower latitudes and higher altitudes and an increase of the Northern Hemisphere zonal wind response by approximately 30%. Moreover, Tomas et al. (2016), Wang et al. (2018), and England et al. (2020) show that the remote effects of sea ice loss on the tropics may depend on the response of the ocean circulation (see also discussion in Screen et al. 2018). Ayres et al. (2022) investigate the impacts of Antarctic sea ice loss on climate and, similarly to Deser et al. (2015), find that the circulation response is larger in coupled experiments than in uncoupled experiments. Screen et al. (2018) suggest that the circulation response to sea ice loss appears to be more consistent between different AOGCMs when compared with AGCMs.

Sea ice loss itself is a response to warming due to greenhouse gas (GHG) emissions. Therefore, coupled model studies that seek to isolate the impacts of sea ice loss, absent other climate forcings, require an additional artificial energy input to be included in the models to melt the sea ice. Various methods to constrain sea ice have been utilized, including surface albedo reduction (Deser et al. 2015; Blackport and Kushner 2016) and the “nudging” and “ghost flux” methodologies, which directly add heat to the sea ice module (Deser et al. 2015; Tomas et al. 2016; Smith et al. 2017; McCusker et al. 2017; England et al. 2020; Peings et al. 2021; see England et al. 2022 for a detailed description of each method and their implementation in AOGCMs). Comparison studies have shown that these methods produce results that are broadly consistent with one another (Screen et al. 2018; Sun et al. 2020). However, England et al. (2022) argue that they also share a common, “spurious” side effect, namely, that the surface temperature response to sea ice loss is overestimated, as the direct warming response to artificial energy input (required to melt the ice) is erroneously included as a response to sea ice loss, when in reality it is the cause.

Support for England et al. (2022)’s argument has been offered by Fraser-Leach et al. (2024), who have developed a technique to correct the response obtained in AOGCMs with constrained sea ice post hoc, using multiparameter pattern scaling. They build on Blackport and Kushner (2017), who decompose the response of some field Z as

$$\delta Z = \frac{\partial Z}{\partial T_l} \Big|_I \delta T_l + \frac{\partial Z}{\partial I} \Big|_{T_l} \delta I, \quad (1)$$

where T_l is the low-latitude SST and I is the sea ice area. The first term represents the response of Z to a change in T_l , absent a change in I , and the second term represents the response of Z to a change in I , absent a change in T_l (i.e., the response that scales with sea ice loss). This equation can be solved for the sensitivities $(\partial Z/\partial T_l)_I$ and $(\partial Z/\partial I)_{T_l}$ given as output from two pairs of experiments, for example, a control experiment, compared against a simulation of climate change with increased GHG emissions, and a simulation where sea

ice is constrained through application of artificial heating to the Arctic. In light of England et al. (2022)’s result that artificial heating drives a spurious warming response, Fraser-Leach et al. (2024) propose that pattern scaling can be adapted to determine the true effect of sea ice loss, which is the component of the response driven by energy input due to changes in the surface albedo associated with reduced sea ice coverage. This is achieved by replacing the scaling variable I with one that accounts for the spurious forcing used to induce sea ice loss (in addition to the ice loss itself).

Considering AOGCM experiments forced by (i) increased GHG emissions and (ii) albedo modification, Fraser-Leach et al. (2024) replace I with the change in net all-sky top-of-atmosphere (TOA) shortwave north of 70°N, SW_{TOA} , which accounts for increased energy input due to reduced sea ice coverage (which reduces the surface albedo), as well as spurious energy input in the albedo modification experiment (due to the fact the ice is artificially darker). Doing so, they find the annual-mean high-latitude warming attributable to sea ice loss is reduced from roughly 8 K when I is used to just over 5 K when SW_{TOA} is used (compared to a total response of roughly 8 K to increased GHG emissions) and the magnitude of the midlatitude zonal wind response is reduced by roughly 50% (while retaining its spatial structure). Noting that Deser et al. (2015) find ocean coupling enhances the midlatitude jet response by roughly 30%, relative to the response in an AGCM, Fraser-Leach et al.’s results imply that the jet response to Arctic sea ice loss could actually be damped, rather than enhanced, by ocean coupling. It is worth noting that artificial heating does not necessarily strengthen all aspects of the climate response to sea ice loss. For example, Lewis et al. (2024) use idealized GCM experiments to show that nudging may artificially weaken the response of Arctic surface temperature persistence to sea ice loss.

The analysis presented in England et al. (2022) is based on simulations run using a dry, diffusive energy balance model (EBM). This choice allows England et al. to compare the surface temperature response to various ice-constraining methods against the true effect of sea ice loss on temperature, which, due to the EBM’s simplicity, can be determined analytically. However, the dry EBM precludes them from assessing the extent to which the spurious, additional warming response is accompanied by artifacts in the response of atmospheric circulation to sea ice loss (which is not represented in the EBM). Additionally, it omits processes important to the real climate system, including the poleward transport of latent heat by water vapor (which can drive polar-amplified warming in the absence of sea ice loss; e.g., Merlis and Henry 2018; Feldl and Merlis 2021), as well as feedbacks associated with clouds (England and Feldl 2024), and the response of poleward heat transport to sea ice loss due to changes in atmospheric circulation (Hwang et al. 2011). Fraser-Leach et al. (2024) extend the analysis of England et al. (2022) to a moist EBM and show that their conclusions are unaltered by this addition. In addition, their pattern scaling approach offers a route to identifying the impacts of spurious warming on the circulation response to sea ice loss in AOGCMs. However, it should be noted that pattern scaling only approximates the true effect of

sea ice loss (compared with an exact quantification in the EBM framework). In addition, [Fraser-Leach et al. \(2024\)](#) have had less success correcting for artificial heat in experiments that use a ghost flux to constrain sea ice, as in this scenario, the appropriate choice for the replacement scaling variable is less clear.

The objective of this study is to extend the work of [England et al. \(2022\)](#) and [Fraser-Leach et al. \(2024\)](#) using the Isca idealized GCM framework ([Vallis et al. 2018](#)), configured as an aquaplanet with a slab ocean and thermodynamic sea ice (similar to that described in [Feldl and Merlis 2021](#); [Chung and Feldl 2024](#)). The true effect of sea ice loss on the climate of the idealized GCM, which we define as the effect of sea ice loss, absent the effect of additional heating required to melt ice, can be obtained by decreasing the freezing point of water to reduce ice coverage. This method does not require surface warming in order to induce sea ice loss. Instead, subfreezing open ocean can exist, and all additional energy input to the climate system arises due to changes in the surface albedo (which occur due to sea ice loss, as opposed to artificial modification of the ice albedo). This methodology is not intended to be physically realizable, but it allows us to isolate the spurious side effects associated with other ice-constraining methods that use artificial heating. Specifically, by comparing the climate response to sea ice loss induced by (i) albedo modification and (ii) a simplified ice-nudging methodology, with that induced by freezing point modification, we are able to isolate the spurious side effects of methodologies (i) and (ii) on surface temperature and large-scale atmospheric circulation in the idealized GCM.

By using a GCM, we are able to capture the response of atmospheric circulation to sea ice loss. This builds upon the representation of atmospheric circulation in EBMs, where the effect of circulation on climate is represented through meridional diffusion of heat (or moist static energy) with a fixed diffusion coefficient. The simplicity of the GCM we use allows us to use freezing point modification to isolate the spurious effects of ice-constraining methods on the climate response to sea ice loss. The idealized GCM thus serves a useful bridge between results obtained using EBMs and studies that use complex AOGCMs. However, our choice to use an idealized model comes at the expense of ocean dynamics, dynamic sea ice, land-sea contrast, the water vapor feedback, and cloud feedbacks, which are all excluded from our model but likely play an important role in mediating the response of the real climate to sea ice loss.

The remainder of this paper is structured as follows. [Section 2](#) presents a description of the idealized GCM we use, and [section 3](#) details our experiment design. Our results are presented in [section 4](#). Finally, discussion and a summary of our main conclusions are included in [section 5](#).

2. Model description

We run numerical experiments using Isca, a framework for modeling the atmospheres of Earth and other planets at varying levels of complexity ([Vallis et al. 2018](#)). The model used for this study constitutes an idealized aquaplanet GCM. It is configured with a semigray radiative transfer scheme, including seasonally varying insolation, and a heavily simplified representation of

moist processes that omits clouds entirely (following [Frierson 2007](#); [O’Gorman and Schneider 2008](#)). The surface is represented as a slab ocean with prescribed ocean heat transport (following [Merlis et al. 2013](#)) and features a simple thermodynamic sea ice code based on [Zhang et al. \(2022\)](#). This configuration is similar to that used by other studies that investigate the climate response to sea ice loss with an idealized model ([Feldl and Merlis 2021](#); [Shaw and Smith 2022](#); [Chung and Feldl 2024](#); [Lewis et al. 2024](#)).

a. Surface energy budget

For ice-free conditions, the model’s surface energy budget evolves according to

$$C \frac{\partial T_{\text{ml}}}{\partial t} = -F_{\text{atm}} + \nabla \cdot \mathbf{F}_{\text{ocean}}, \quad (2)$$

$$T_s = T_{\text{ml}}, \quad (3)$$

where T_{ml} is the ocean mixed layer temperature, T_s is the surface temperature, F_{atm} denotes the net downward radiative and turbulent surface heat flux, and $\nabla \cdot \mathbf{F}_{\text{ocean}}$ represents the prescribed poleward ocean heat transport. The $C = \rho_w c_w d$ is the heat capacity of the mixed layer ocean, where $\rho_w = 1035 \text{ kg m}^{-3}$ is the density of seawater; $c_w = 3989 \text{ J kg}^{-1} \text{ K}^{-1}$ is the specific heat capacity of water; and $d = 30 \text{ m}$ is the depth of the mixed layer (chosen to obtain a seasonal cycle of surface temperature with a realistic amplitude and lag relative to the seasonal cycle of insolation).

When the surface temperature drops below the freezing temperature T_{freeze} , sea ice is allowed to grow, and the surface energy budget is given by

$$C \frac{\partial T_{\text{ml}}}{\partial t} = -F_{\text{base}} + \nabla \cdot \mathbf{F}_{\text{ocean}}, \quad (4)$$

$$L \frac{\partial h}{\partial t} = F_{\text{atm}} - F_{\text{base}}, \quad (5)$$

$$F_{\text{base}} = F_0(T_{\text{ml}} - T_{\text{freeze}}), \quad (6)$$

$$F_{\text{atm}} = F_i \equiv k_i \frac{T_{\text{freeze}} - T_s}{h}. \quad (7)$$

This representation of thermodynamic sea ice is based on the “zero layer” model proposed by [Semtner \(1976\)](#), and our implementation exactly follows that described by [Zhang et al. \(2022\)](#). Here, h is the sea ice thickness and F_{base} is the basal heat flux from the mixed layer into the ice, which linearly depends on the difference between T_{ml} and the temperature at the ice base (the melting temperature, which for simplicity we set equal to T_{freeze}). When ice is present, the surface temperature increment ΔT_s is determined implicitly via a balance between F_{atm} and F_i , the conductive heat flux through the ice, i.e.,

$$F_{\text{atm}} + \frac{dF_{\text{atm}}}{dT_s} \Delta T_s = F_i + \frac{dF_i}{dT_s} \Delta T_s, \quad (8)$$

unless this procedure yields $T_s > T_{\text{freeze}}$. In this scenario, Eqs. (7) and (8) are replaced with $T_s = T_{\text{freeze}}$ (representing surface

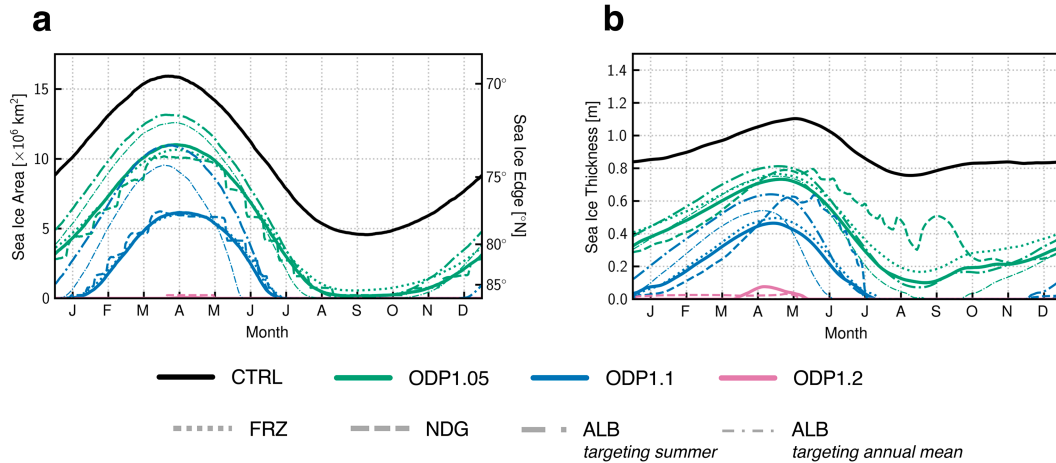


FIG. 1. Seasonal cycle of Northern Hemisphere (a) SIA and (b) SIT obtained in idealized GCM experiments. Solid lines show the CTRL experiment and ODP experiments, and broken lines show experiments with SIA constrained to match that obtained in the ODP experiments. The color indicates correspondence between ODP and ice-constrained simulations. Dashed lines show SIA in NDG experiments, dotted lines show SIA in FRZ experiments (FRZ3.75, FRZ5, and FRZ10), and dash-dotted lines show SIA in ALB experiments. For ALB experiments, thicker dotted lines show experiments that best match the summer (JJA) SIA in the corresponding ODP runs (ALB.48 and ALB.35), and thinner lines show experiments that best match the annually averaged SIA (ALB.45 and ALB.1). The FRZ10 is ice-free all year-round and therefore is not visible in either panel.

melt). Here, the coefficient F_0 is set to $120 \text{ W m}^{-2} \text{ K}^{-1}$, the thermal conductivity of ice is set to $k_i = 2 \text{ W m}^{-1} \text{ K}^{-1}$, and the latent heat of fusion is set to $L = 3 \times 10^8 \text{ J m}^{-3}$. For our control simulation, we set $T_{\text{freeze}} = -2^\circ\text{C}$ (roughly the freezing point of salt-water) to ensure a realistic latitude for the ice edge (see Fig. 1a). The mean sea ice thickness (SIT) obtained in our control simulation, shown in Fig. 1b, is a little low relative to observations and reanalysis (Schweiger et al. 2011; Kwok 2018) but does fall within the range simulated by CMIP6 models for the present day (Chen et al. 2023; Winkelbauer et al. 2024).

Surface-atmosphere energy exchange is given by

$$F_{\text{atm}} = SW_s + LW_s - L_v E - S, \quad (9)$$

where SW_s and LW_s are the net downward shortwave and longwave radiative fluxes at the surface, respectively; E is the evaporative flux; and S is the sensible heat flux. The latent heat of vaporization of water is set to $L_v = 2.5 \times 10^6 \text{ J Kg}^{-1}$. These terms are computed by the radiative transfer and boundary layer codes implemented in the model, as described in the following subsections. It is important to note that F_{atm} has an explicit dependence on T_s through LW_s and the surface turbulent fluxes; if this were not the case, then it would not be necessary to write Eq. (7) in the implicit form given by Eq. (8).

Finally, a semirealistic, time-invariant representation of ocean heat transport is included in the model, using the functional form described by Merlis et al. (2013):

$$\nabla \cdot \mathbf{F}_{\text{ocean}} = \frac{Q_0}{\cos \vartheta} \left(1 - \frac{2\vartheta^2}{\vartheta_0^2} \right) \exp\left(-\frac{\vartheta^2}{\vartheta_0^2}\right), \quad (10)$$

where ϑ is the latitude, $\vartheta_0 = \pm 16^\circ$, and we set the amplitude to be $Q_0 = 30 \text{ W m}^{-2}$. This functional form is intended to

approximate an estimate of annually and zonally averaged ocean heat transport obtained from NCEP reanalysis data (Bordoni 2007).

b. Radiative transfer

Radiative transfer is represented using a simplified semi-gray scheme with fixed optical depths (similar to Frierson et al. 2006; Frierson 2007; O’Gorman and Schneider 2008). For longwave (infrared) radiation, upward and downward fluxes are computed using the two-stream approximation:

$$\frac{dF_{\text{lw}}^\uparrow}{d\tau_{\text{lw}}} = F_{\text{lw}}^\uparrow - \sigma_{\text{sb}} T^4, \quad (11)$$

$$\frac{dF_{\text{lw}}^\downarrow}{d\tau_{\text{lw}}} = \sigma_{\text{sb}} T^4 - F_{\text{lw}}^\downarrow, \quad (12)$$

where $\sigma_{\text{sb}} = 5.67 \times 10^{-8} \text{ W m}^{-2} \text{ K}^{-4}$ is the Stefan-Boltzmann constant, T is the temperature, and τ_{lw} is the longwave optical depth, defined by the function

$$\tau_{\text{lw}} \equiv [f\sigma + (1-f)\sigma^4][\tau_e + (\tau_p - \tau_e)\sin^2 \vartheta], \quad (13)$$

where $f = 0.2$, $\sigma = p/p_s$ is the pressure normalized by the surface pressure, τ_e is the longwave optical depth at the equator, and τ_p is the longwave optical depth at the pole. For our control experiment, we set $\tau_e = 7.2$ and $\tau_p = 3.6$. At the top of atmosphere, $F_{\text{lw,TOA}}^\downarrow = 0$, and at the lower boundary, $F_{\text{lw,sfc}}^\uparrow = \sigma_{\text{sb}} T_s^4$. The net longwave surface flux in Eq. (9) is then given by $LW_s = F_{\text{lw,sfc}}^\downarrow - \sigma_{\text{sb}} T_s^4$.

For shortwave (visible light) radiation, the downward flux is given by

TABLE 1. Summary description of idealized aquaplanet GCM experiments. The base configuration used for each experiment is described in section 2. Modifications to this configuration specific to each experiment are described.

Experiment	Intervention	Notes
CTRL	None	Model configuration is described in section 2.
ODP	Longwave optical depth increase	Longwave optical depth is increased by a multiplicative prefactor so that $\tau_{\text{lw}} = \tau_{\text{lw,ctrl}} \times \text{ODP}$. We consider three values, $\text{ODP} = 1.05, 1.1,$ and 1.2 . Experiments run with these values are denoted as ODP1.05, ODP1.1, and ODP1.2, respectively.
FRZ	Freezing point modification	Sea ice loss is induced by reducing the freezing point of water, T_{fz} . This method does not require additional energy input to melt ice. Experiments are run for a wide range of T_{freeze} (see section 3). The experiments with $T_{\text{freeze}} = -3.75^\circ, -5^\circ,$ and -10°C , denoted as FRZ3.75, FRZ5, and FRZ10, respectively, yield annually averaged SIAs that best match those of ODP1.05, ODP1.1, and ODP1.2, respectively.
NDG_NC	Nudging	Sea ice loss induced by applying heating to the sea ice at latitudes and times where it is not present in the target climate [see Eq. (16)]. NDG experiments target the SIA obtained in the ODP experiments and are denoted as NDG_NC1.05, NDG_NC1.1, and NDG_NC1.2.
NDG	Nudging	As above, but with a corrective cooling applied in regions where sea ice loss does not occur so that the globally averaged energy input due to nudging is zero. Three experiments are run: NDG1.05, NDG1.1, and NDG1.2.
ALB	Albedo modification	Sea ice loss is induced by reducing the ice albedo. Experiments are run for a wide range of α_{ice} (see section 3). Experiments with $\alpha_{\text{ice}} = 0.45$ and 0.1 , denoted as ALB.45 and ALB.1, obtain annually averaged SIAs that best match those in ODP1.05 and ODP1.1, respectively. Experiments with $\alpha_{\text{ice}} = 0.48$ and 0.35 , denoted as ALB.48 and ALB.35, obtain JJA SIAs that best match those in ODP1.05 and ODP1.1, respectively. We were unable to replicate the degree of sea ice loss obtained in ODP1.2 using any value of $\alpha_{\text{ice}} \geq 0.1$ ($\alpha_{\text{ocean}} = 0.1$ is the value for the surface albedo of the ice-free ocean).

$$F_{\text{sw}}^{\downarrow} = (1 - \alpha_{\text{TOA}})S_{\text{TOA}} \exp(-\tau_{\text{sw}}\sigma^2), \quad (14)$$

where $\tau_{\text{sw}} = 0.22$ is the shortwave optical depth and $1 - \alpha_{\text{TOA}} \equiv [0.75 + 0.15 \times P_2(\sin\theta)]$ is a latitudinally varying coalbedo, which is included to account for the missing effect of clouds. The top-of-atmosphere insolation S_{TOA} is computed for a circular orbit and Earth's obliquity, excluding the diurnal cycle and assuming a solar constant of $S_0 = 1360 \text{ W m}^{-2}$. All shortwave radiation reflected at the surface is assumed to immediately escape to space so that $F_{\text{sw}}^{\uparrow}(\tau_{\text{sw}}) = \alpha_{\text{sfc}} F_{\text{sw,sfc}}^{\downarrow}$, where α_{sfc} is the surface albedo. The net shortwave surface flux in Eq. (9) is given by $\text{SW}_s = (1 - \alpha_{\text{sfc}})F_{\text{sw,sfc}}^{\downarrow}$. Open ocean ($h = 0$) has an albedo of $\alpha_{\text{ocean}} = 0.1$, and for our control simulation, we set the albedo of sea ice ($h > 0$) to $\alpha_{\text{ice}} = 0.55$. The dependence of α_{sfc} on h introduces an implicit dependence of α_{sfc} on T_s .

c. Subgrid-scale processes

Simplified representations of subgrid-scale processes are included in the model, exactly following O'Gorman and Schneider (2008). Convection is parameterized using the "simple Betts–Miller" scheme of Frierson (2007), incorporating the modifications to shallow convection implemented by O'Gorman and Schneider (2008). A gridscale condensation scheme is included to adjust humidity and temperature whenever there is large-scale saturation of a grid box (i.e., relative

humidity exceeding 100%). Boundary layer turbulence is parameterized using a k -profile scheme similar to Troen and Mahrt (1986). Surface fluxes of sensible and latent heat, i.e., S and $L_v E$ in Eq. (9), and momentum are computed using standard bulk aerodynamic formulas [Eqs. (9)–(11) in Frierson et al. 2006]. Drag coefficients are obtained from Monin–Obukhov similarity theory, using the implementation described by O'Gorman and Schneider (2008).

d. Dynamical core

Isca uses the Geophysical Fluid Dynamics Laboratory spectral dynamical core to integrate the primitive equations forward in time. For the present study, we configure the model with a T42 spectral resolution, corresponding to a latitude–longitude resolution of roughly 2.5° , and a time step of 900 s. In the vertical, there are 30 layers, distributed according to $\sigma = \exp[-5(0.05\tilde{z} + 0.95\tilde{z}^3)]$, where \tilde{z} is evenly spaced on the unit interval (following Frierson et al. 2006).

3. Experiment design

a. Control experiment and "climate change" experiments

Table 1 summarizes the various experiments we run using the idealized GCM. For our control simulation, denoted CTRL, we run the model using the parameters defined in the

previous subsections for 50 years, starting from an isothermal, quiescent initial condition. The final 20 years of this simulation are used for analysis. In addition, we run three climate change experiments, where the longwave optical depth is increased by a multiplicative prefactor, optical depth parameter (OPD): $\tau_{lw} = \tau_{lw,ctrl} \times ODP$. We consider three values, $ODP = 1.05, 1.1, \text{ and } 1.2$, which yield sea ice responses ranging from partial sea ice loss to nearly year-round total sea ice loss (Fig. 1). The global mean surface temperature increases obtained in these experiments are $\Delta T_s = 1.5, 2.8, \text{ and } 4.4$ K, respectively. These experiments are denoted ODPX, where X indicates the value of ODP used. Each ODP experiment is run for 50 years, using the start of the 31st year of the CTRL simulation as an initial condition. The final 20 years of each ODP experiment are used for analysis.

b. Sea ice loss experiments

To investigate the impacts of sea ice loss on climate, we run a suite of “counterfactual” experiments with constrained sea ice, absent other climate forcings. We consider experiments with a modified freezing temperature for ice, which capture the true effect of sea ice loss on the model climate, alongside a simplified implementation of nudging, and albedo modification [targeting both summer sea ice area (SIA) and annually averaged SIA], which are commonly used methodologies for constraining sea ice in AOGCMs. Each approach is described in detail in the subsections that follow. For all sea ice loss experiments, we set $ODP = 1$ and use the start of the 31st year of the CTRL simulation as an initial condition, and are run for 50 years, with the final 20 years used for analysis. Seasonally varying, zonally averaged SIA and SIT are shown in Fig. 1 for selected experiments with constrained sea ice, compared against the CTRL and ODP runs. To confirm that 20 years of data are sufficient for our study, we conducted additional analysis of our simulations using 10-yr subsets drawn from the final 20 years of each run and found that our main results are insensitive to this alteration.

1) FREEZING POINT MODIFICATION

Our choice to configure Isca with a slab ocean and thermodynamic sea ice means that we can induce sea ice loss by reducing the freezing temperature T_{freeze} in the thermodynamic sea ice code. This method allows us to reduce the sea ice area without directly inducing surface warming. Annual-mean warming in these experiments is driven by changes in the surface albedo due to sea ice loss, which we define as the true effect of sea ice loss (consistent with England et al. 2022; Fraser-Leach et al. 2024). We have checked this by configuring the model so that the albedos of open ocean and sea ice are the same; in this configuration, the annually and zonally averaged surface temperature is insensitive to T_{freeze} . We note it would also be possible to design experiments where the optical depth is increased (as in the ODP experiments), and then, T_{freeze} is increased to target SIA in the CTRL simulation. It is possible that this approach would yield a “different true effect” of sea ice loss due to nonlinear interactions between increased temperatures (due to increased optical depth) and

sea ice. We choose to reduce sea ice area relative to CTRL using freezing point reduction because this approach is analogous to that used in comprehensive climate models where SIA is reduced using nudging or albedo modification.

We have run experiments using the following values for the freezing point: $T_{freeze} = -2.5^\circ, -3^\circ, -3.5^\circ, -3.75^\circ, -4^\circ, -5^\circ, -6^\circ, \text{ and } -10^\circ\text{C}$. In the CTRL configuration, $T_{freeze} = -2^\circ\text{C}$ to ensure a realistic value for the ice edge; this is our reason for beginning this sequence of counterfactual experiments with $T_{freeze} = -2.5^\circ\text{C}$. We label these experiments freeze X (FRZX), where X indicates the magnitude $|T_{freeze}|$ used. The experiments FRZ3.75, FRZ5, and FRZ10 yield annually averaged SIAs that best match those of the ODP1.05, ODP1.1, and ODP1.2 experiments, respectively. Seasonally varying SIA and SIT obtained from the FRZ3.75, FRZ5, and FRZ10 experiments are shown using dotted lines in Fig. 1. This figure demonstrates that these experiments accurately capture the seasonal cycle of SIA loss in the ODP experiments, in addition to recovering the correct annual-mean value. These experiments also adequately capture the response of SIT although it is slightly underestimated for the ODP1.05 simulation.

We note that it would be difficult to implement this methodology using a more sophisticated model, featuring a dynamic ocean and dynamic sea ice, as it would require an artificial extrapolation of the equation of state for water to subfreezing temperatures. Additionally, in more complex climate models, sea ice has been shown to influence annually averaged surface temperatures through pathways that do not depend on the ice–albedo feedback. Specifically, sea ice (i) warms the Arctic, through net latent energy transport into the Arctic associated with sea ice export; and (ii) suppresses a summer lapse-rate feedback, due to warm summer temperatures that arise over ice due to its small effective heat capacity (Hahn et al. 2022). In our model, pathway (i) is excluded because our model does not represent dynamic ice transport and pathway (ii) is suppressed because we use a prescribed longwave optical thickness that does not depend on water vapor content or clouds, thus weakening surface temperature increase during summer and consequently the summer lapse-rate feedback.

2) ALBEDO MODIFICATION

For our albedo modification experiments, we vary the sea ice albedo, α_{ice} . We consider the following values: $\alpha_{ice} = 0.5, 0.485, 0.48, 0.475, 0.45, 0.4, 0.35, 0.3, 0.2, 0.15, \text{ and } 0.1$ (i.e., the same value as α_{ocean}). These experiments are denoted as albedo X (ALBX), where X indicates the value of α_{ice} used.

Reducing the sea ice albedo has a limited effect during the polar night and is therefore most effective at reducing summer SIA. This means that the seasonal cycle of sea ice loss under albedo modification is skewed toward summer months, and a choice must be made regarding whether to target the summer sea ice loss or annually averaged sea ice loss due to climate change (Blackport and Kushner 2016; Sun et al. 2020; England et al. 2022). Through our parameter sweep over α_{ice} , we cover both options. The ALB.45 and ALB.1 experiments obtain the annually averaged SIA that best matches that in

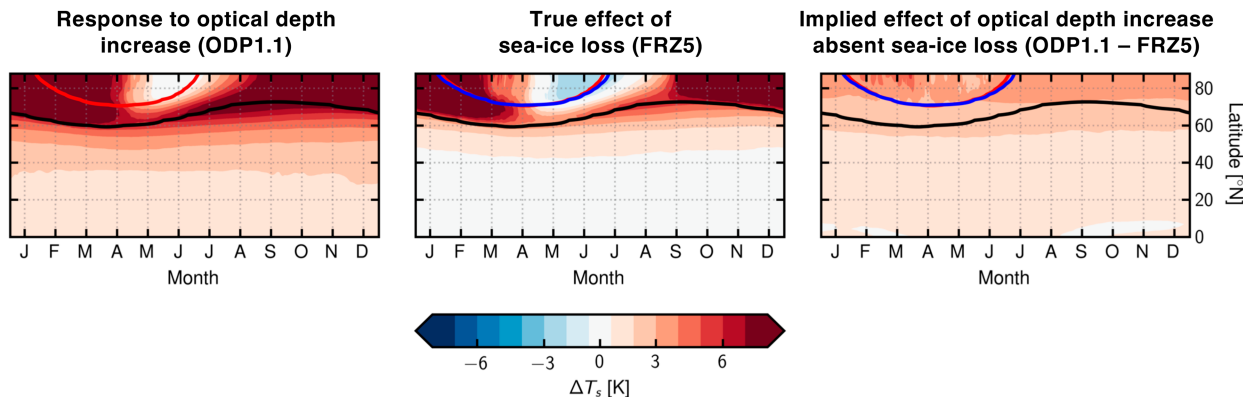


FIG. 2. Seasonal surface temperature response obtained in the ODP1.1 and FRZ5 experiments (which obtains an SIA that matches that of ODP1.1; see Fig. 1). (left) Difference between ODP1.1 and CTRL experiments. (center) Difference between FRZ5 and CTRL experiments, which represents the true contribution of sea ice loss to the response in ODP1.1. (right) Difference between ODP1.1 and FRZ5, which represents the implied effect of increasing optical depth, minus the effect of sea ice loss. Red, blue, and black lines represent the sea ice edge in the ODP1.1, FRZ5, and CTRL experiments, respectively.

the ODP1.05 and ODP1.1 experiments, respectively. The seasonal cycle of SIA in ALB.45 and ALB.1 is presented in Fig. 1 as thin dash-dotted lines, showing how targeting annually averaged SIA leads to excessive sea ice loss in summer and restricted sea ice loss in winter (compared with the corresponding ODP experiments). ALB.48 and ALB.35 yield the best match to the summer sea ice loss obtained in ODP1.05 and ODP1.1, respectively. These experiments are shown in Fig. 1 as thick dash-dotted lines, revealing a much better match to the onset of summer sea ice loss, at the expense of more severely underrepresenting sea ice loss in winter. We note that we were unable to replicate the degree of sea ice loss obtained in the ODP1.2 experiment using any of the values for α_{ice} listed above.

3) NUDGING

Finally, we run the model in the CTRL configuration but with the sea ice area nudged toward that obtained in each of the ODP experiments described above.

Nudging is implemented by adding an additional term to the equation for sea ice thickness evolution [Eq. (5)]:

$$L \frac{\partial h}{\partial t} = \dots + F_{nudge}, \quad (15)$$

which is nonzero at latitudes and times when sea ice is present, but $h_{target} = 0$, where h_{target} is the target sea ice distribution (a function of latitude and day of year, obtained from one of the ODP experiments described above). In the present study, we use a simple implementation of F_{nudge} following England et al. (2022), given by

$$F_{nudge.nc} = \begin{cases} -Lh/\tau & \text{when } h_{target} = 0, \\ 0 & \text{otherwise,} \end{cases} \quad (16)$$

where $\tau = 86400s$ is chosen for the nudging time scale. This approach adds energy to the system; to correct for this, we include an additional, constant correction term, $F_{correct}$. This

term is included at grid points where $F_{nudge.nc} = 0$, with the magnitude of $F_{correct}$ set to that which ensures the global, area-weighted average of

$$F_{nudge} = F_{nudge.nc} + F_{correct} \quad (17)$$

is zero ($F_{correct}$ is computed at each time step). We note that while this approach achieves no net energy input from the nudging process, it does so by introducing an unphysical cooling effect to low latitudes.

Experiments including the correction described above are referred to using the name nudge X (NDGX), and experiments with no correction are referred to using NDG_NCX, where X indicates the value of ODP used in the simulation from which h_{target} is derived. The seasonal cycle of SIA obtained from the NDGX experiments is shown with dashed lines in Fig. 1a, demonstrating that the simple nudging implementation adequately constrains SIA to match each ODP experiment. The seasonal cycle of sea ice in the NDG_NCX experiments is essentially identical to that in the NDGX runs. We note that the NDG experiments underestimate the reduction of SIT in summer (i.e., ice that remains too thick). This is due to the simplified implementation of nudging we use, which only constrains SIA. We will show later that the spurious response to nudging-induced sea ice loss is a direct response to the artificial heating F_{nudge} . If SIT were constrained in the NDG experiments in addition to SIA, this would require a larger F_{nudge} , and so we expect that the spurious side effects of nudging would be enhanced.

4. Results

a. True effect of sea ice loss on idealized model climate

We begin by describing the true effect of sea ice loss on surface temperature and atmospheric circulation in the idealized GCM, using the ODP1.1 and FRZ5 experiments as an illustrative example. Figure 2 shows the seasonally varying

response of zonally averaged surface temperature obtained with each experiment, relative to CTRL, as well as their difference (ODP1.1–FRZ5). In ODP1.1, the surface temperature response is polar amplified, with ΔT_s exceeding 8 K in polar regions ($>70^\circ\text{N}$) for much of the year, compared with more modest warming of roughly 3 K in midlatitudes and 1.5 K in the tropics. In the Arctic, the surface temperature response is suppressed in late spring and early summer (from May through July) compared with the rest of the year. At lower latitudes, there is far less seasonal variation in the response. This seasonal cycle of polar amplification is consistent with that obtained in more sophisticated climate models (Lu and Cai 2009; Hahn et al. 2021; Chung et al. 2021; Liang et al. 2022) and identified in observations (Screen and Simmonds 2010a).

Comparison between the ODP1.1 and FRZ5 experiments shows that in our idealized GCM, the majority of polar warming in ODP1.1, as well as its seasonality, is attributable to sea ice loss. However, the residual warming (ODP1.1–FRZ5), which quantifies the implied effect of increasing optical depth, absent the effects of sea ice loss, is still polar amplified, consistent with previous work using idealized models (Merlis and Henry 2018; Feldl and Merlis 2021). In the tropics, the residual warming is comparable to the total warming in ODP1.1, which indicates that it is primarily a direct response to increasing optical depth, as opposed to being an effect of sea ice loss.

It is interesting to note that between May and July, polar regions in the FRZ5 experiment experience cooling relative to the CTRL experiment. This cooling arises because summer sea ice retreat occurs earlier in the year in the FRZ5 experiment, compared with CTRL. During this period, surface temperature increase is temporarily halted, as energy input at the surface is used to melt ice instead. This effect can be identified in Fig. 3, which shows the seasonal cycle of polar surface temperature for the CTRL and FRZ5 experiments. The fact that this “latent heating effect” is manifest as a cooling in FRZ5, instead of an absence of warming, might appear to be an unphysical artifact of the freezing point modification methodology. However, we do not believe this to be the case, as it is necessary for cooling to occur in FRZ5 in summer if the residual warming obtained from ODP1.1–FRZ5 is to remain polar amplified throughout the year, as is expected in an idealized, cloud-free GCM (Merlis and Henry 2018; Feldl and Merlis 2021; England and Feldl 2024). We note that Chung and Feldl (2024) also find sea ice loss to be associated with cooling in early summer, using an alternative methodology (which does not involve freezing point modification).

Figure 4 shows the response of the zonally averaged atmospheric temperature, zonal wind, and meridional eddy heat flux to sea ice loss in FRZ5. The top row shows the annual mean response, and the middle and bottom rows show the response in DJF and JJA, respectively. The response of atmospheric temperature is polar amplified and strongest in the lower troposphere (below $p \approx 700$ hPa). It is greatest in winter and weaker in summer, as was the case for surface temperature. Turning to diagnostics for the atmospheric circulation, we observe that the poleward flank of the eddy-driven jet is weakened in response to sea ice loss, throughout the depth of

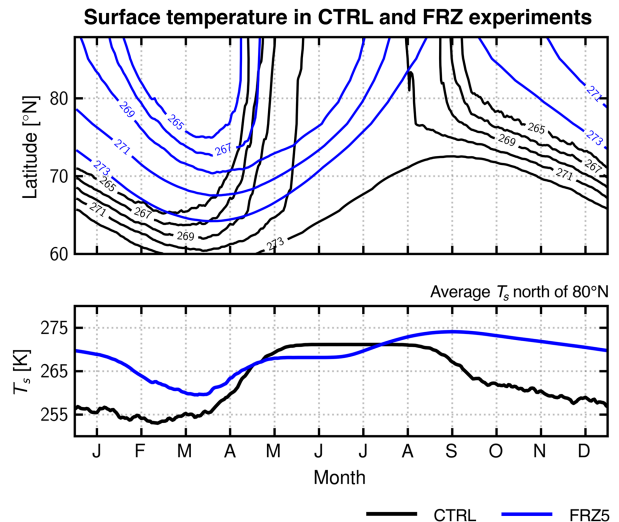


FIG. 3. Surface temperature obtained in the CTRL (black) and FRZ5 (blue) experiments. The freezing temperature for CTRL is $T_{\text{freeze}} = 271.15$ K and that for FRZ5 is $T_{\text{freeze}} = 268.15$ K. Surface temperature increase in summer is slowed by the latent heating required to melt sea ice. Sea ice retreat occurs earlier in the year for the FRZ5 sea ice loss experiment compared with CTRL. This causes the surface temperature in FRZ5 to be briefly cooler than in CTRL (between May and July; see Fig. 2, center panel).

the troposphere. In the upper troposphere, the jet is additionally strengthened at the edge of the subtropics (i.e., the upper-tropospheric jet core is shifted equatorward). The weakening of the eddy-driven jet is accompanied by a weakening of the storm tracks, inferred using the meridional eddy heat flux as a proxy. As with atmospheric temperature, the zonal wind response in the lower troposphere and the storm-track response are at their greatest in winter. These features are generally consistent with results from AGCMs (Smith et al. 2022) as well as coupled AOGCMs (Screen et al. 2018). The zonal wind response in the upper troposphere displays less seasonality but is the strongest in summer.

We note that increasing optical depth in gray-radiation GCMs tends to induce an equatorward jet shift, even in the absence of sea ice loss, which is counter to expectations from more sophisticated models (Tan et al. 2019; Davis and Birner 2022). Davis and Birner (2022) attribute this effect to the absence of shortwave radiative heating by ozone in the lower stratosphere. This results in climatological zonal winds over the pole that are too weak (i.e., there is no polar vortex). Davis and Birner suggest this inhibits the poleward shift of eddies with fast phase speeds and thus the poleward shift of the eddy-driven jet. Due to this deficiency, we do not discuss the circulation response to increasing optical depth as part of our analysis and instead focus solely on the response to sea ice loss (spurious or otherwise). We would not expect the mechanism proposed by Davis and Birner (2022) to inhibit the direct response of the circulation to sea ice-induced warming in the lower troposphere. However, the absence of a well-resolved stratosphere (and any significant stationary waves) in our model will suppress the stratospheric response pathway

True effect of sea-ice loss on circulation (FRZ5)

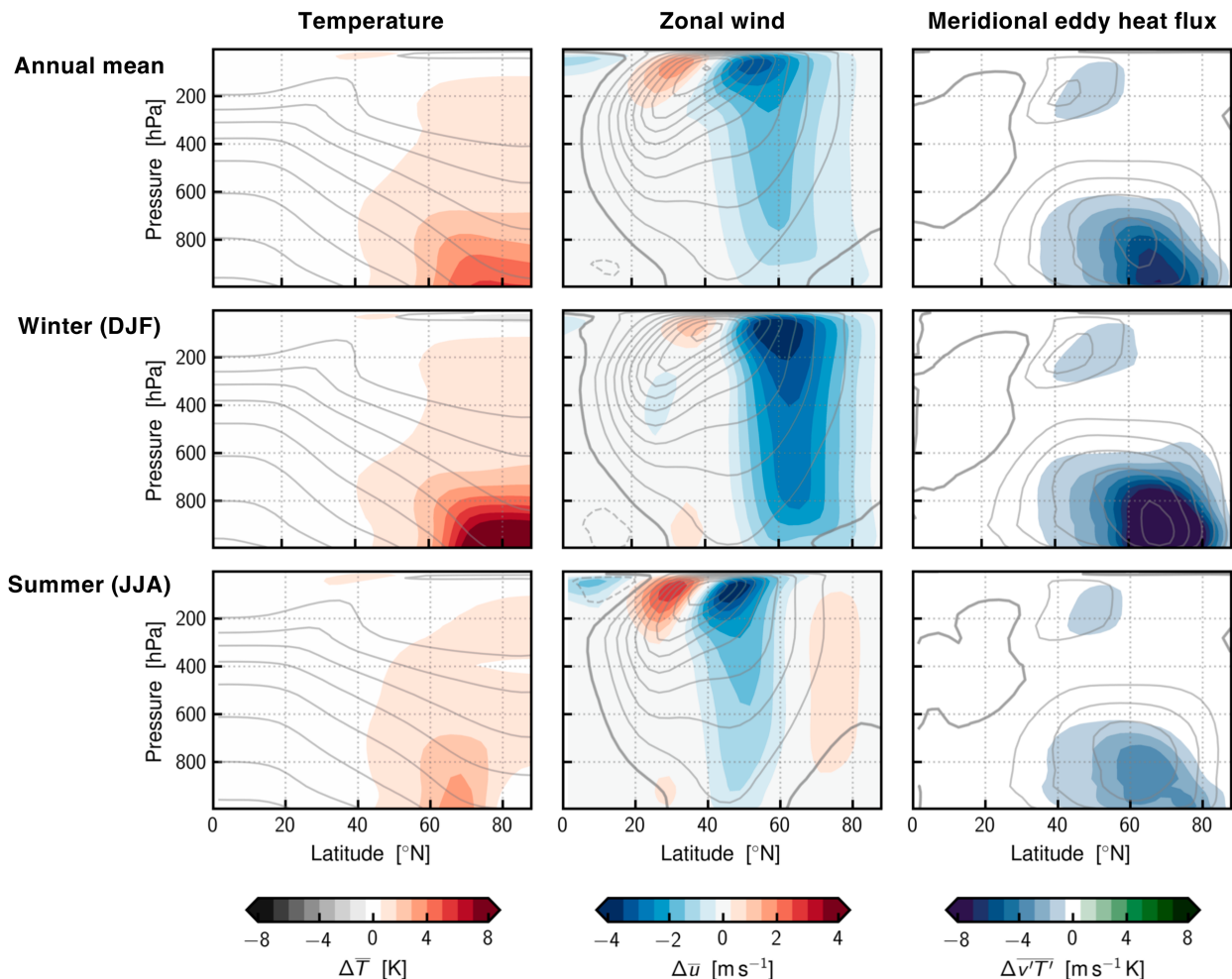


FIG. 4. Response of the zonally averaged circulation to sea ice loss obtained in the FRZ5 experiment. (top) Annual mean response, (middle) response in winter (DJF), and (bottom) response in summer (JJA). (left) Atmospheric temperature, (center) zonal wind, and (right) meridional eddy heat flux $v'T'$, which we use here as a measure of storm-track intensity. In each panel, the response obtained from taking the difference between FRZ5 and CTRL is shown with color contours, and the climatology obtained with CTRL is shown with solid contours. Solid contours have increments of 10 K for temperature (beginning at 300 K), 5 m s^{-1} for zonal wind (with the zero contour marked in bold), and $5 \text{ m s}^{-1} \text{ K}$ for the eddy heat flux (with the zero contour marked in bold).

(see, e.g., Screen et al. 2018). This may weaken the total circulation response to sea ice loss in our model.

b. Spurious effects of ice-constraining methods on surface temperature

1) ANNUAL MEAN RESPONSE

Area-averaged annual-mean surface temperature responses obtained in each of our experiments, relative to the CTRL experiment, are shown in Fig. 5. Figure 5a shows the response of globally averaged surface temperature, and Fig. 5b shows the response of polar-averaged surface temperature (latitudes $> 70^\circ\text{N}$). In each panel, the temperature response is plotted as a function of the sea ice edge on the lower x axis. This is related to the

response of SIA (see caption), denoted as ΔSIA , which is shown on the upper x axis. Plotting against the sea ice edge (or ΔSIA) allows for a fairer comparison between experiments that achieve differing degrees of sea ice loss.

For a given change in SIA, the smallest globally averaged surface temperature response is obtained by the NDG (pink) and FRZ (true effect of sea ice loss; green) experiments. For NDG and FRZ, the additional, globally averaged energy input that causes global-mean warming is solely due to the surface albedo response to sea ice loss (for NDG, this is achieved using the correction term described in section 3b). By contrast, the ALB (light blue) and NDG_NC (yellow) experiments include an additional, spurious energy input in the global mean, which results in enhanced global warming. This

Surface temperature response to sea-ice loss

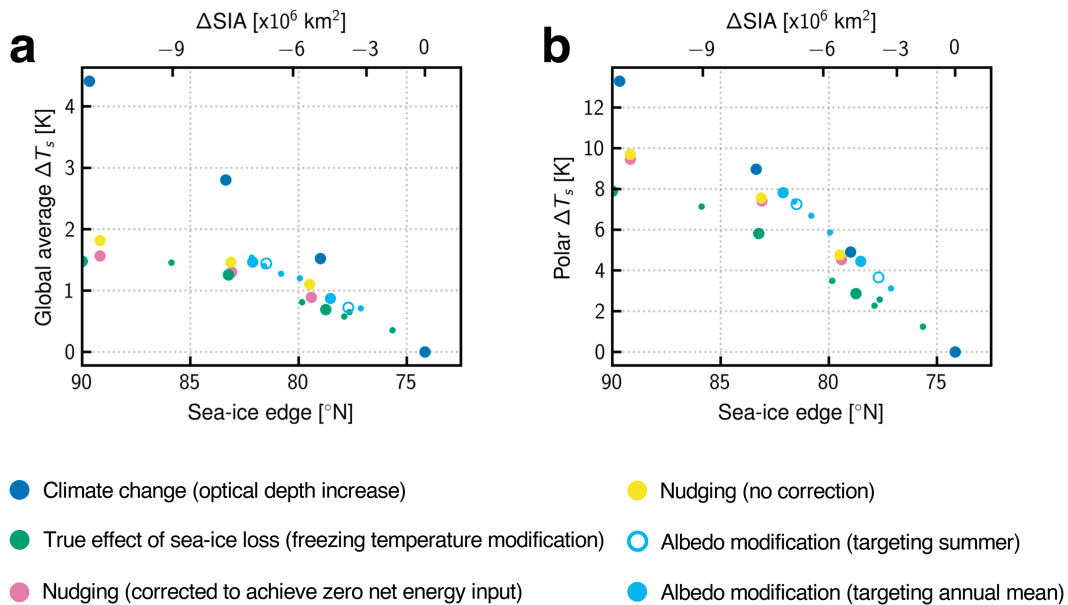


FIG. 5. Surface temperature response to sea ice loss as a function of the sea ice edge latitude. (a) Annual-mean, globally averaged surface temperature and (b) annual-mean, polar-averaged temperature (latitudes $> 70^{\circ}\text{N}$). ΔSIA (relative to CTRL) is also shown on the upper x axes. SIA is related to the sea ice edge latitude via $\text{SIA} = 2\pi a^2 (1 - \sin\theta_{\text{ice}})$, where a is Earth's radius. Ice-constrained experiments that best match the SIA obtained in ODP experiments are plotted using a larger marker size. Specifically, the ODP1.1 experiment and associated ice-constrained experiments (analyzed extensively in the remainder of this paper) are those with larger markers and $-9 \times 10^6 \text{ km}^2 \leq \Delta\text{SIA} \leq -6 \times 10^6 \text{ km}^2$. In both panels, the CTRL experiment is shown at $(\Delta\text{SIA}, \Delta T) = (0, 0)$ (using the same color as for the ODP experiments).

spurious global-mean energy input represents the energy required to melt the sea ice, which itself induces warming. In the corrected NDG experiment, this energy is “borrowed” from the tropics instead, while in FRZ, no global-mean energy input is required to induce sea ice loss.

Figure 5b shows that the polar surface temperature response in the nudging and albedo modification experiments is comparable to the total surface temperature response due to climate change (ODP experiments; dark blue) and significantly greater than that obtained in the freezing point modification experiments. This difference represents a spurious polar warming effect arising from the nudging and albedo modification methodologies. It arises as each of ALB, NDG, and NDG_NC requires surface temperature to be raised above freezing to induce sea ice loss, before any warming caused by sea ice loss actually occurs. As such, the polar surface temperature response in ALB, NDG, and NDG_NC represents the combined response to sea ice loss, plus the energy input required to induce sea ice loss. It is interesting to note that the albedo modification experiments targeting summer SIA (hollow light blue points in Fig. 5) obtain globally averaged and polar-averaged ΔT_s of a similar magnitude to the albedo modification experiments targeting annually averaged SIA (filled light-blue points) and still overestimate warming compared to the FRZ experiments. Ultimately, annual-mean warming in the albedo modification experiments is primarily

driven by the shortwave radiative transfer response $\Delta\text{SW}_{\text{toa}}$. This response is similar irrespective of whether summer or annual-mean SIA is targeted, due to the limited influence of sea ice on the TOA energy budget during the winter (constrained to be zero during the polar night).

Figure 6 shows the latitudinal structure of the annual-mean response of surface temperature [panel (a)] and surface enthalpy [panel (b)], as well as the additional energy input [relative to CTRL; panel (c)], for the ODP1.1 experiment and the constrained sea ice experiments that target SIA in ODP1.1. The surface enthalpy is the prognostic variable at the model's surface. It is defined by

$$E = \begin{cases} -Lh & \text{when } h > 0, \\ C(T_s - T_{\text{freeze}}) & \text{when } h = 0, \end{cases} \quad (18)$$

where h is the sea ice thickness, T_s is the surface temperature, T_{freeze} is the freezing point of ice, L is the latent heat of fusion, and C is the heat capacity of the ocean mixed layer (see section 2).

As identified in section 4a, the surface temperature response in the ODP1.1 experiment is strongly polar amplified and maximal at the pole. Strong polar amplification occurs because much of the idealized model's climate sensitivity is due to feedbacks associated with sea ice loss (there are no radiative feedbacks associated with moisture or clouds, for

Latitudinal structure of response (targeting ODP1.1)

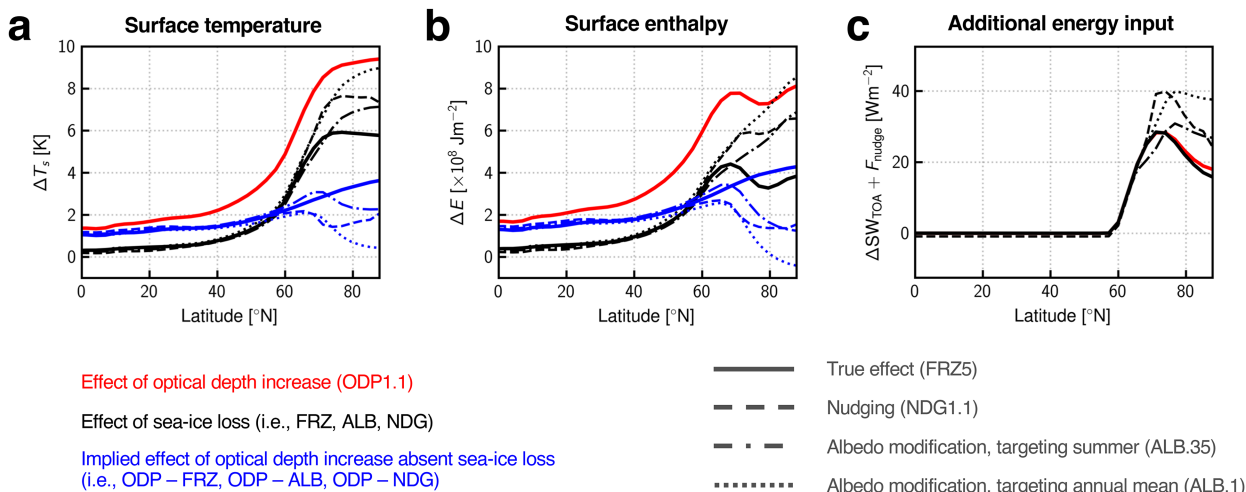


FIG. 6. Latitudinal structure of annual-mean response obtained in ODP1.1 and corresponding runs with constrained sea ice. (a) Response of surface temperature, (b) response of surface enthalpy, and (c) additional energy input for each experiment (relative to CTRL), which is the sum of net TOA shortwave response and F_{nudge} (F_{nudge} is only nonzero for NDG1.1). The thick red curves show the response to increasing optical depth (ODP-CTRL), the thick black curves show the true effect of sea ice loss obtained from the FRZ5 experiment (FRZ-CTRL), and the thick blue curves show the response of the ODP experiment minus the effect of sea ice loss (ODP-FRZ). Broken black and blue lines show an equivalent decomposition for the nudging and albedo modification methodologies [using NDG1.1, ALB.35 (targeting summer), and ALB.1 (targeting annual mean)].

example). This effect is amplified by the high sensitivity of the sea ice edge to climate change (this is a feature of aquaplanet GCMs with thermodynamic sea ice, for example, CESM2; England et al. 2024, manuscript submitted to *Environ. Res. Climate*). Consequently, much of the polar-amplified warming ($\Delta T_s \approx 6$ K) is attributed to sea ice loss by the FRZ5 experiment (solid black line) although the residual warming (solid blue line) is still polar-amplified. In terms of the surface enthalpy, the response in the ODP1.1 experiment has a secondary peak at the ice edge (Fig. 6b, red line). This is collocated with the latitude where the additional energy input due to the effect of sea ice loss on albedo is maximized (Figs. 6b,c, solid black lines). This peak is not present in the surface temperature response, demonstrating that some of the additional energy input has gone into melting ice instead of increasing surface temperature.

Each of the experiments that constrain sea ice while keeping T_{freeze} unchanged relative to CTRL (NDG1.1, ALB.35, and ALB.1) overestimate the surface temperature response to sea ice loss when compared with FRZ5 (cf. the broken black lines with the solid black line in Fig. 6a). A consequence of this is that the implied warming due to increasing optical depth (broken blue lines) has an unphysical structure that peaks in midlatitudes, before decreasing toward the pole. In the case of the ALB.1 experiment, which targets annually averaged SIA using albedo modification, this effect is pronounced enough that the residual warming due to increasing optical depth alone is polar-deamplified, which is a clear indicator that too much warming is being attributed to sea ice loss by this methodology. This effect is reduced in the ALB.35 experiment because this experiment targets summer sea ice loss,

which, by definition, underestimates SIA change compared with other ice-constrained experiments.

Figure 6c shows that the nudging and albedo modification experiments include a spurious additional energy input, beyond that which occurs in response to sea ice loss in either ODP1.1 or FRZ5. This is the spurious energy input required to melt the ice in the absence of either an increase in optical depth or a modification of the freezing temperature. In the case of the albedo modification experiments, it is the largest at the pole. This has the effect of masking the midlatitude local maximum in the surface enthalpy response (compared to the response in FRZ5) and causes the surface temperature response to sea ice loss to be maximally overestimated at the pole. For the nudging experiment, the spurious additional energy input is more evenly distributed over polar latitudes ($>70^\circ\text{N}$), which is mirrored by a more even overestimation of the surface enthalpy response in Fig. 6b. These results are broadly consistent with those obtained by England et al. (2022) using a dry EBM.

2) SEASONAL CYCLE

To further illustrate the spurious effects of ice-constraining methods on surface temperature, we now examine the seasonal cycle of the temperature response to sea ice loss obtained in the nudging and albedo modification experiments that target SIA in ODP1.1. This is shown in Fig. 7. At first glance, each method appears to capture a similar warming response to sea ice loss, compared to the true effect, which is large in autumn, winter, and early spring but suppressed in summer (Fig. 7, left-hand side column). However, upon

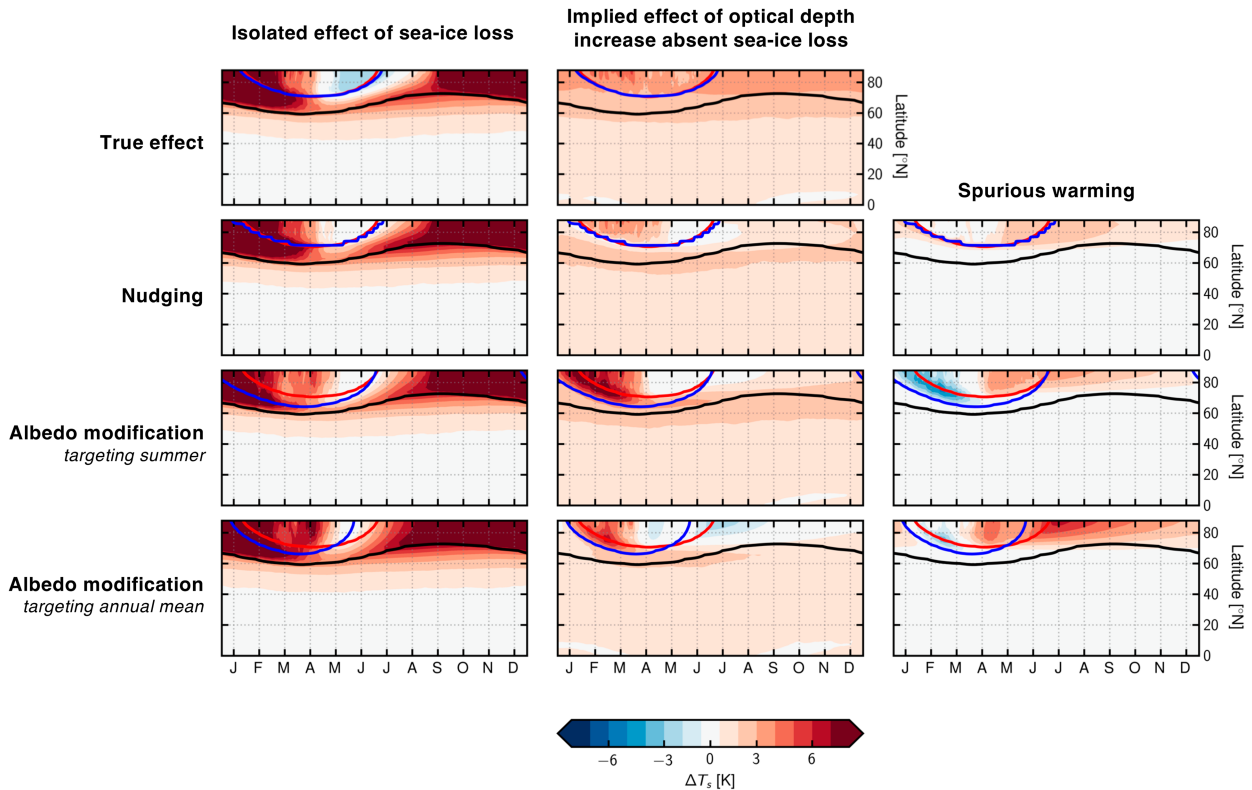


FIG. 7. Spurious effects of ice-constraining methods on surface temperature. (left) Surface temperature response relative to CTRL in experiments targeting sea ice loss in ODP1.1 [FRZ5, NDG1.1, ALB.35 (targeting summer), and ALB.1 (targeting annual mean)]. (center) Difference between the total response and the response obtained in constrained sea ice experiments (e.g., ODP–NDG). (right) Spurious warming from the ice-constraining method, computed as the difference in surface temperature between each experiment targeting ODP1.1 and the experiment FRZ5 (e.g., NDG–FRZ). Red, blue, and black lines represent the sea ice edge in the ODP1.1, constrained sea ice (i.e., FRZ, NDG, or ALB, as appropriate), and CTRL experiments, respectively. The data shown in the top row are reproduced from Fig. 2.

taking the difference between the response obtained in each of NDG1.1, ALB.35, and ALB.1 and the true response obtained from FRZ5, it can be identified that each of the ice-constraining methods overestimates the temperature response to sea ice loss during the late summer and early winter (Fig. 7, right-hand side column). The albedo modification experiments additionally underestimate the response to sea ice loss during early spring. Consequently, in NDG1.1, ALB.35, and ALB.1, the implied warming in the absence of sea ice loss (Fig. 7, central column) exhibits an unphysical seasonality which cannot be explained by any of the physical processes included in the idealized GCM. This unphysical seasonality is not present when the true effect of sea ice loss is isolated using freezing point modification (Fig. 2, right panel) or consistent with the results of previous work (Hahn et al. 2022; Chung and Feldl 2024).

The spurious additional energy input in each of these experiments is shown in Fig. 8. For the nudging experiment, the additional term in Eq. (15) causes additional energy input during winter and early spring, in order to prevent sea ice from growing beyond the target SIA. This energy initially goes into warming the mixed layer, which subsequently

becomes ice-covered, and it is only when sea ice retreat occurs in summer that the additional energy input manifests as spurious increase in surface temperature. By contrast, albedo modification has no effect on the top-of-atmosphere energy balance during the polar night, which means that spurious additional energy input occurs later in the year (relative to the nudging experiment), in late spring and early summer. However, because the spurious energy input occurs when the surface is already ice covered, the temperature response to this forcing emerges at the surface immediately and is then communicated to the mixed layer via the conductive heat flux through the ice. Consequently, both nudging and albedo modification cause spurious warming that is greatest in summer despite the fact that spurious energy input occurs at different times of the year.

As noted above, the albedo modification experiments additionally underestimate the surface temperature response during late winter. This effect arises because these experiments retain too much sea ice during winter, relative to the target climate change experiment. When sea ice is present, the effective heat capacity of the surface is reduced (Hahn et al. 2022), which causes the surface temperature to cool more in winter than would be the case if it were ice-free.

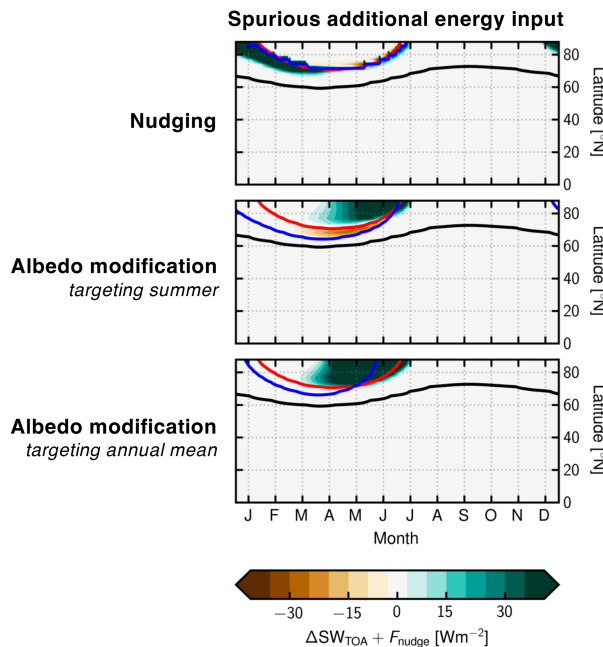


FIG. 8. Spurious additional energy input obtained in the NDG1.1, ALB.35, and ALB.1 experiments. This is computed as the sum of the net TOA shortwave response and F_{nudge} , minus the shortwave response in experiment FRZ5 (the true effect of sea ice loss). Red, black, and blue lines show the sea ice edge, as in Fig. 7.

c. Impact on large-scale atmospheric circulation

In this section, we analyze the spurious impacts of the nudging and albedo modification methodologies on the circulation response to sea ice loss.

1) ANNUAL- AND ZONAL-MEAN CIRCULATION RESPONSE

Figure 9 shows the annual-mean response of the zonally averaged circulation to sea ice loss for the nudging and albedo modification experiments that target SIA obtained in the ODP1.1 experiment, relative to CTRL, as well as the difference between each response and the true effect of sea ice loss (e.g., NDG1.1–FRZ5). The left-hand side column shows atmospheric temperature, the central column shows the zonal wind, and the right-hand side column shows the meridional eddy heat flux, $\overline{v'T'}$ (the overline denotes a zonal and day-of-year average, and primes indicate departures therefrom), which we use as a simple measure of storm-track intensity.

For each experiment, the spurious temperature response in Fig. 9 has a magnitude similar to that obtained for surface temperature (see, e.g., Fig. 6a, comparing the broken and solid black lines). It is mostly confined to the lower troposphere ($p \gtrsim 700$ hPa), and at greater altitude, the spurious temperature response is weak compared to the total response. It is notable that the “mini global warming” response to sea ice loss obtained in AOGCMs with constrained sea ice (Deser et al. 2015) cannot be identified in Fig. 9. In AOGCMs, the influence of sea ice loss on the tropics is driven by the response

of ocean dynamics (Tomas et al. 2016; Wang et al. 2018; England et al. 2020), which cannot occur in the idealized GCM as it is configured using a slab ocean with prescribed ocean heat transport.

Due to spurious warming, the nudging and albedo modification experiments overestimate the response of the zonal-mean zonal wind to sea ice loss. This effect is relatively pronounced for the NDG1.1 and ALB.1 experiments, where there is a spurious additional weakening of the zonal wind around 65°N. The spurious component of the zonal wind response is roughly barotropic and near the surface accounts for approximately 35% of the total response to sea ice loss. In addition to the zonal wind, nudging and albedo modification also drive a spurious additional weakening in storm-track activity, measured using the meridional eddy heat flux. As with the temperature response, this effect is mostly confined to the lower troposphere and is relatively weak compared with the total response to sea ice loss suggested by each method.

2) STORM-TRACK RESPONSE

To analyze the spurious effects of nudging and albedo modification on the storm track in greater detail, we consider an additional metric for storm-track activity, namely, the “storm-track intensity” I introduced by Shaw et al. (2018). Storm-track intensity is defined by

$$I(\vartheta) = 2\pi a \cos\vartheta F_{\text{TE}}(\vartheta), \quad (19)$$

where $F_{\text{TE}} = \overline{v'm'}$ is the meridional eddy moist static energy (MSE) flux. The MSE itself is given by $m = c_p T + gz + Lq$, where T is the temperature, z is the geopotential height, q is the specific humidity, c_p is the specific heat capacity of dry air, and g is the acceleration due to gravity.

Figure 10 shows the response of storm-track intensity, ΔI , to sea ice loss for the FRZ, NDG, and ALB experiments, relative to CTRL, plotted against the latitude of the sea ice edge. In this figure, ΔI is integrated vertically (mass weighted) over the depth of the atmosphere and meridionally averaged between 30° and 60°N. As with the eddy heat flux shown in Fig. 9, sea ice loss drives a decrease in storm-track intensity, which is enhanced in the nudging and albedo modification experiments compared with the true response to sea ice loss due to spurious energy input.

Using the MSE budget framework described by Shaw et al. (2018) and Shaw and Smith (2022), it is possible to derive an equation for the spurious response of the storm-track intensity, ΔI^* , to spurious energy input, $\Delta I_{\text{input}}^*$, associated with the nudging and albedo modification methodologies (see the appendix for derivation; asterisks indicate a spurious forcing or response):

$$\Delta I^* = \Delta I_{\text{LW}}^* - \Delta I_M^* + \Delta I_{\text{input}}^*, \quad (20)$$

where $\Delta I_{\text{LW}}^* = 2\pi a^2 \int_{\pi/2}^{\vartheta} \Delta \text{LW}_{\text{TOA}} \cos\vartheta d\vartheta$ is the spurious longwave cooling response, where LW_{TOA} is the net downward top-of-atmosphere longwave radiative flux and $\Delta I_M^* = 2\pi a \cos\vartheta \Delta F_M(\vartheta)$ is the spurious response of heat transport by the

Spurious effects of ice-constraining methods on circulation (annual mean)

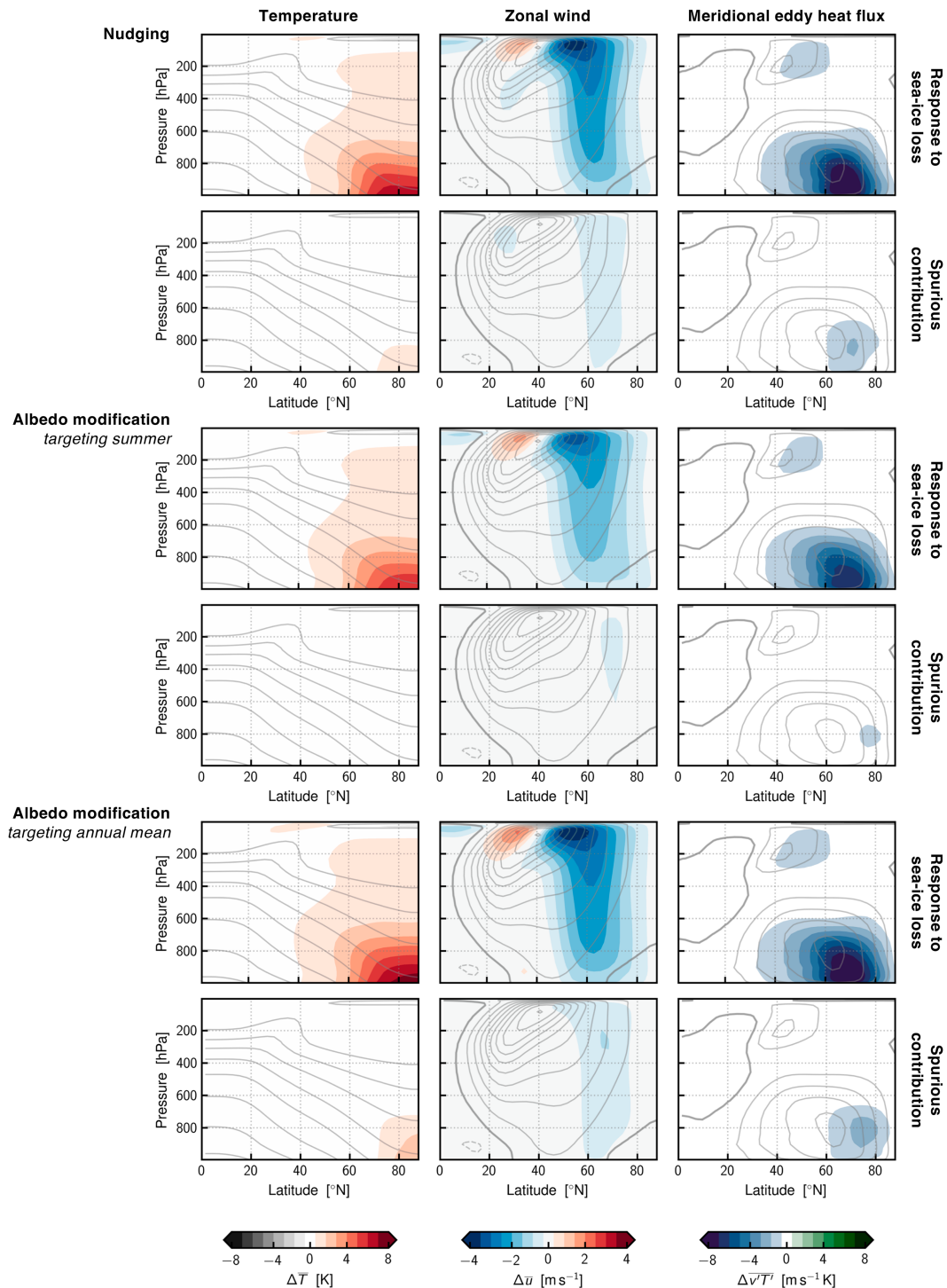


FIG. 9. Annually averaged effect of sea ice loss on circulation for experiments targeting SIA in the ODP1.1 experiment. For each variable, the response to sea ice loss is computed relative to the CTRL experiment, and the spurious response is computed relative to the FRZ5 experiment. Solid contours show the climatology obtained with the CTRL experiment (see Fig. 4 caption for more information).

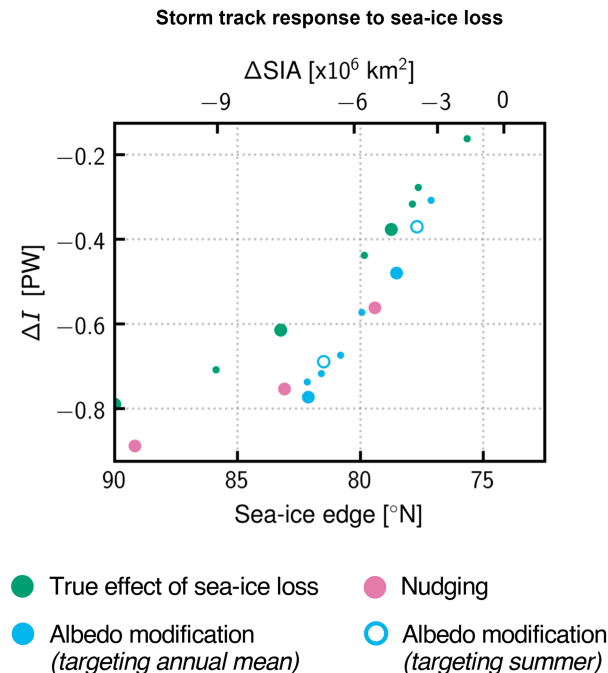


FIG. 10. Storm-track response to sea ice loss, quantified using the storm-track intensity I [Eq. (19)]. Ice-constrained experiments that best match the target SIA obtained in the ODP1.05, ODP1.1, and ODP1.2 experiments are plotted using a larger marker size.

mean flow, where $F_M = \overline{v\bar{m}}$. To compute the spurious responses ΔI_{LW}^* and ΔI_M^* , the differences ΔLW_{TOA} and ΔF_M are taken between sea ice loss experiments with additional heat (i.e., NDG and ALB) and the FRZ experiment that captures the true response (absent additional heat). The spurious forcing ΔI_{input}^* is given by

$$\Delta I_{input}^* = 2\pi a^2 \int_{\pi/2}^{\theta} (F_{nudge} - \Delta\alpha_{sfc} F_{sw,sfc}^{\downarrow}) \cos\theta d\theta, \quad (21)$$

where nonzero $\Delta\alpha_{sfc}$ between the ALB and FRZ experiments is entirely spurious (e.g., due to artificial darkening of the ice). Equation (20) predicts that changes in storm-track intensity are due to changes in the meridional flux divergence implied by spurious energy input, integrated over latitude (Shaw and Smith 2022).

Figure 11 shows the spurious forcing ΔI_{input}^* (green) and the spurious responses $-\Delta I_M^*$ (pink), ΔI_{LW}^* (orange), and ΔI^* (blue), obtained by taking the difference between the nudging and albedo modification experiments targeting SIA in ODP1.1, and the true effect of sea ice loss in ODP1.1 (given by FRZ5). In each case, the MSE framework shows that spurious forcing, ΔI_{input}^* , drives a spurious storm-track response, ΔI^* , of a similar magnitude. The storm-track response is partially offset by an increase in radiative cooling, ΔI_{LW}^* , in response to spurious forcing, but amplified by a weakening of the midlatitude mean meridional circulation (Ferrel cell), which transports heat equatorward in midlatitudes. As the Ferrel cell is eddy driven (Vallis 2017), this effect could be interpreted as an eddy

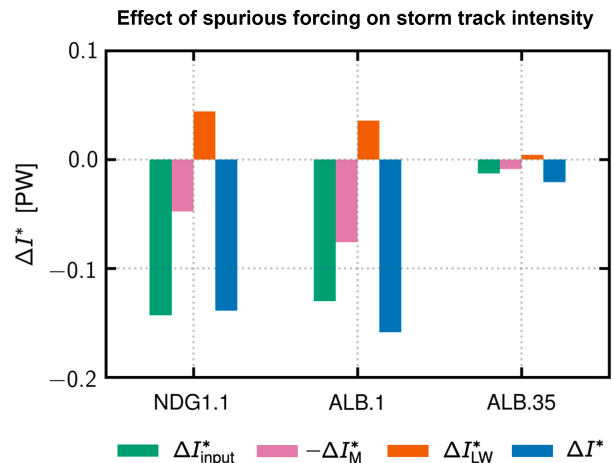


FIG. 11. Response of different terms in the MSE intensity budget to spurious forcing in the NDG1.1, ALB.1, and ALB.35 experiments. The green bar shows the spurious forcing, the pink bar shows the response of the mean meridional circulation MSE intensity, the orange bar shows the response of radiative cooling, and the blue bar shows the response of eddy MSE intensity. All quantities are meridionally averaged between 30° and 60°N.

feedback, whereby the initial weakening of transient eddies in response to spurious energy input causes a weakening of the mean meridional circulation, which subsequently drives a further response in the transient eddies.

3) ZONAL-MEAN CIRCULATION RESPONSE IN JJA

Finally, we consider how the spurious effects of ice-constraining methods on circulation vary with the seasonal cycle. Figure 12 shows the same information as Fig. 9 but now averaged over boreal summer (JJA) as opposed to the whole year. In the FRZ5 experiment, the response of atmospheric circulation in summer was found to be weaker than the response in either the annual mean or winter (see Fig. 4). This is less apparent in the NDG and ALB experiments because the spurious circulation response in these experiments is larger in summer compared with the annual mean (consistent with the surface temperature response discussed in section 4b). This causes the total JJA circulation response to sea ice loss to be substantially overestimated.

As with surface temperature (see Fig. 7), the spurious atmospheric temperature responses in Fig. 12 are largest at the pole and offset from the true temperature response (Fig. 4) which is greatest at around 70°N in summer. As a result, the JJA meridional temperature gradient is weakened in the nudging and albedo modification experiments poleward of 70°N, whereas in FRZ5, it is slightly enhanced. This drives a spurious weakening of the zonal-mean zonal wind around 70°N, masking the true effect of sea ice loss, which actually strengthens the zonal wind at high latitudes in FRZ5 in JJA. As with the zonal wind response, the nudging and albedo modification experiments overestimate the meridional eddy heat flux response, with a spurious contribution that is larger in summer compared with the annual mean. At the surface,

Spurious effects of ice-constraining methods on circulation (JJA)

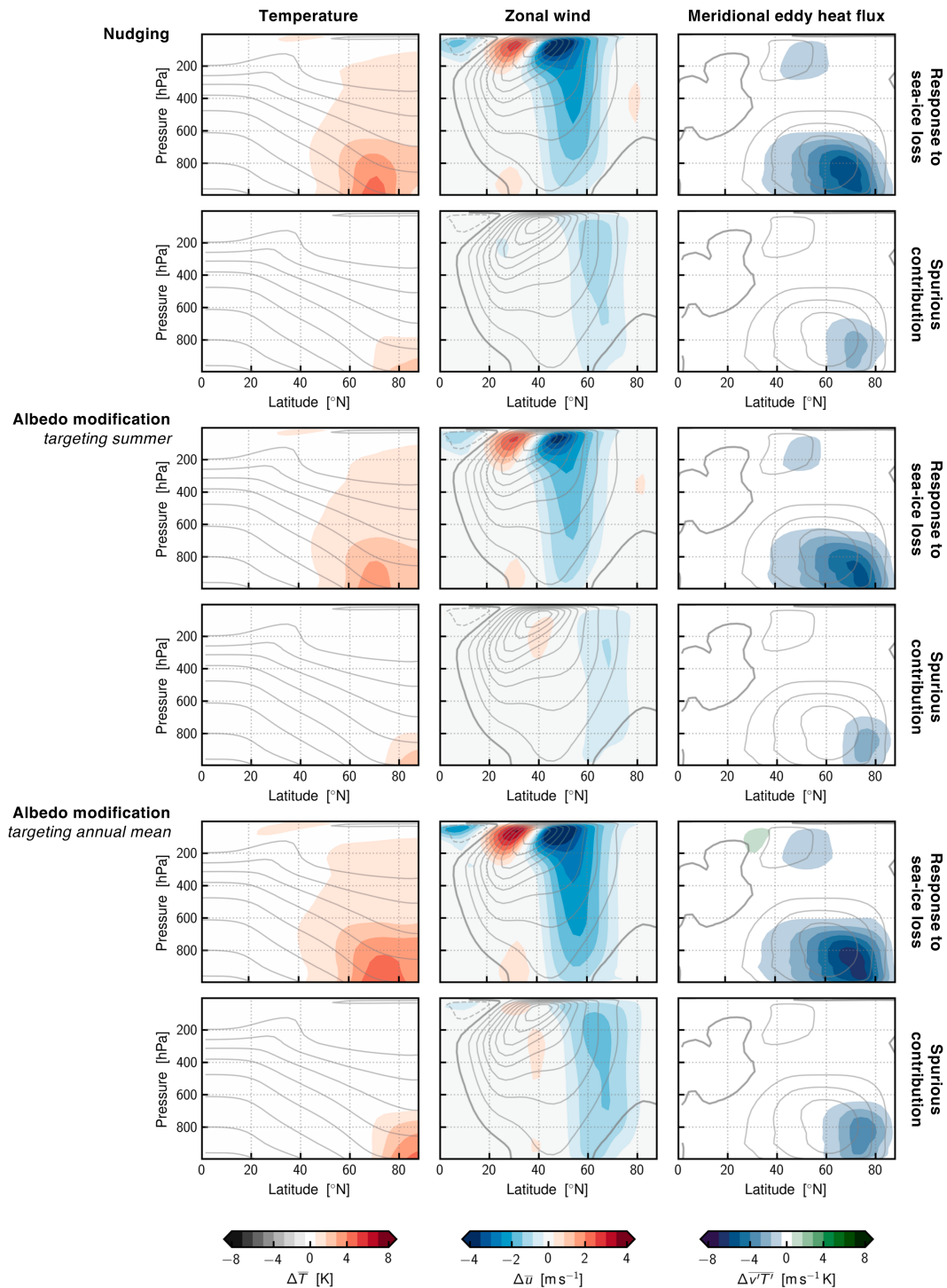


FIG. 12. Effect of sea ice loss atmospheric circulation in summer (JJA), for experiments targeting SIA in the ODP1.1 experiment. For each variable, the response to sea ice loss is computed relative to the CTRL experiment, and the spurious response is computed relative to the FRZ5 experiment. Solid contours show the JJA climatology obtained with the CTRL experiment (see Fig. 4 caption for more information).

this effect accounts for roughly 45% of the total response to sea ice loss obtained in the NDG1.1 and ALB.1 experiments.

5. Conclusions and discussion

In this study, we have analyzed the effect of sea ice loss on the climate of an idealized GCM with thermodynamic sea ice. We use three methods to constrain sea ice: freezing point modification, which isolates the true response to sea ice loss in our model, i.e., the response obtained without using artificial energy input to melt ice, and nudging and albedo modification, which are commonly used methods for constraining sea ice in fully coupled AOGCMs (see, e.g., Sun et al. 2020).

We show that nudging and albedo modification cause too much warming in response to sea ice loss when compared with the true effect isolated using freezing point modification (e.g., Fig. 5a). This arises because the surface temperature response to sea ice loss induced using these methods includes a spurious contribution that is a direct effect of the energy input required to melt sea ice, rather than an effect of sea ice loss itself. We find that spurious warming is most prominent in polar regions, where in the most extreme cases, it causes the temperature response to sea ice loss to be comparable to the total temperature response to climate change (Figs. 5b and 6a). Analysis of these cases would attribute no polar warming to other factors (e.g., GHG emissions). This arises as the spurious additional energy input associated with nudging, and to a greater extent albedo modification, increases with latitude toward the pole (Fig. 6c). These results confirm and extend those presented by England et al. (2022) and Fraser-Leach et al. (2024). We additionally show that spurious warming associated with both nudging and albedo modification is maximal in boreal summer, in spite of the fact that the true temperature response to sea ice loss is at its greatest in boreal winter (Fig. 2b).

Using freezing point modification, we show that the true effect of sea ice loss on circulation in our idealized GCM primarily consists of a weakening of the zonal-mean zonal wind on the poleward flank of the midlatitude jet, accompanied by a strengthening on the equatorward flank of the jet in the upper troposphere, and a weakening of the midlatitude storm track (Fig. 4). This response is greatest in winter when the effect of sea ice loss on surface temperature is greatest. Spurious warming in nudging and albedo modification experiments leads to an overestimation of the circulation response to sea ice loss compared to the true effect (Fig. 9). Using the MSE budget framework proposed by Shaw et al. (2018) and Shaw and Smith (2022), we show that spurious weakening of storm-track intensity occurs in response to a reduction in the divergence of radiative and nonatmospheric energy fluxes, implied by spurious energy input at high latitudes (Fig. 10). As with the temperature response, we find that the effect of spurious energy input on the circulation is greatest in boreal summer (Fig. 12). In some sense, this is a desirable result, given that most interest is in the wintertime, when the response to sea ice loss is believed to be largest (Deser et al. 2010).

Our results suggest that coupled AOGCMs that use nudging or albedo modification to constrain Arctic sea ice may overestimate the response of temperature and circulation,

particularly during boreal summer where the circulation response contains a large spurious contribution (Fig. 12). However, it is important to note that our results will be sensitive to the idealized model configuration we use. In particular, the omission of key climate processes, such as the cloud and water vapor radiative feedbacks, means that the ice-albedo feedback has an outsized influence on the climate of the idealized model. Further, we note that our model does not exhibit a prominent “mini global warming response,” identified in studies that use coupled AOGCMs (Deser et al. 2015), and specifically, there is little warming in any of our experiments in the tropical free troposphere. This likely arises because our model does not include a dynamic ocean (Tomas et al. 2016; Wang et al. 2018; England et al. 2020). Therefore, we cannot comment on the extent to which this tropical response is a “real” effect of coupling, or a spurious effect of the methods used to constrain sea ice in AOGCMs.

Given these limitations, separating the “true effect” of sea ice loss from the spurious effects of nudging and albedo modification in sophisticated AOGCMs remains an important topic for future research. Unfortunately, freezing point modification cannot be trivially implemented in AOGCMs, as it would require modification of the equation of state used in either the ocean or sea ice component of the model. Nevertheless, it is worth noting that our albedo and freezing point modification experiments yield roughly the same globally averaged, and polar-averaged, surface temperature responses as a function of the change in top-of-atmosphere shortwave, ΔSW_{TOA} , which is shown in Fig. 13. A similar result is obtained for the storm-track intensity, shown in Fig. 14. This suggests an alternate strategy for albedo modification in AOGCMs, namely, targeting the total effect of sea ice loss on albedo, instead of sea ice area or volume itself, which in our simplified model would yield the true temperature response to sea ice loss.

As discussed in the introduction, Fraser-Leach et al. (2024) suggest that multiparameter pattern scaling can be utilized to correct for spurious heating in AOGCM simulations that use albedo modification to constrain sea ice. This is achieved by defining the climate response to sea ice loss so that it scales with SW_{TOA} instead of sea ice area. The fact that the response to sea ice loss in our FRZ (true effect) and ALB experiments collapses onto the same curve, when plotted as a function of ΔSW_{TOA} , supports this choice.

However, this methodology also has some limitations. First, Fraser-Leach et al. show that their method is not exact; specifically, by applying their methodology to the EBM used by England et al. (2022), they find that the surface temperature response corrected for artificial heat approaches the known true response to sea ice loss in the EBM but does not equal it. The magnitude of spurious warming is underestimated at high latitudes, and notably, this issue appears to become worse when moisture is included in the model (≈ 0.5 K underestimation in the dry EBM compared with ≈ 1 K in the moist EBM). Additionally, the seasonal cycle of spurious warming isolated using this methodology is greatest in winter, rather than summer (Luke Fraser-Leach, personal communication), which is inconsistent with the results obtained using our idealized model, as well as the fact that albedo modification causes spurious energy input in summer (which should immediately warm the ice

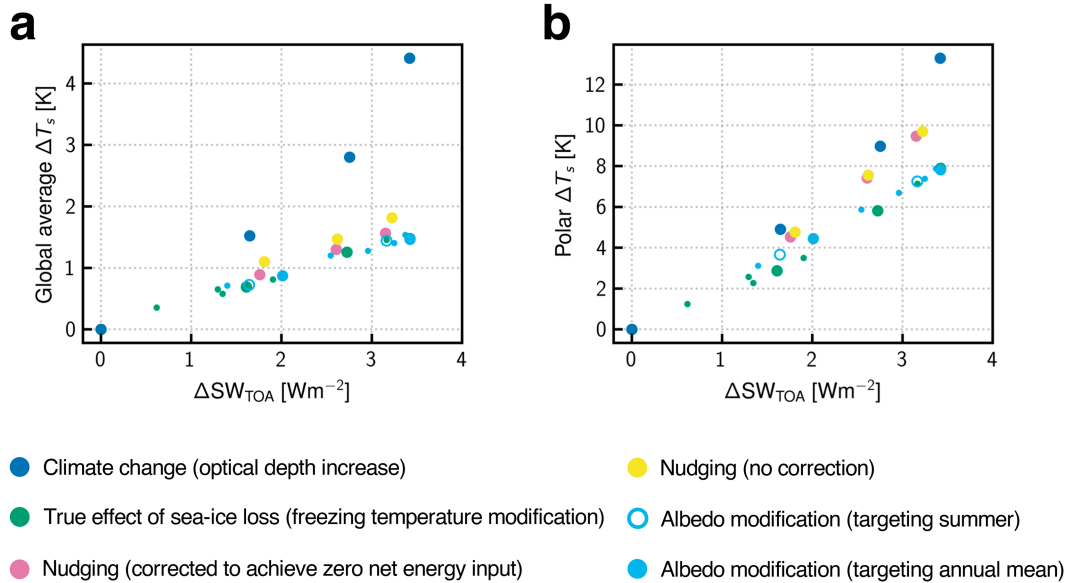
Surface temperature response vs. ΔSW_{TOA} 

FIG. 13. Surface temperature response to sea ice loss as a function of the change in globally averaged net TOA shortwave radiation. (a) Annual-mean, globally averaged surface temperature and (b) annual-mean, polar-averaged temperature (latitudes $> 70^\circ\text{N}$). As in Fig. 5, but for ice-constrained experiments that best match the SIA obtained in ODP experiments that are plotted using a larger marker size.

surface temperature). While beyond the scope of this study, we believe it would be useful to test the pattern scaling approach using the idealized model experiments we have presented. Finally, Fraser-Leach et al. note that F_{TOA} is a less appropriate

choice for the scaling variable when correcting for artificial heat in AOGCM simulations that use methods other than albedo modification and that the “correct” choice for an alternative scaling variable is not immediately obvious. This problem is evident in Figs. 13b and 14, where the nudging experiments exhibit too great a response as a function of ΔSW_{TOA} . This is because ΔSW_{TOA} does not account for the spurious energy that is input by the nudging methodology at high latitudes.

In this paper, we have focused on the spurious impacts of ice-constraining methods on the response of coupled AOGCMs to sea ice loss. However, it is worth considering the implications of our results, as well as those of England et al. (2022) and Fraser-Leach et al. (2024), for studies that make use of AGCMs with prescribed SST and SIC. Whether AGCM experiments contain a spurious contribution will depend on whether the SST prescribed in regions of sea ice loss is attributable to sea ice loss itself or if it is actually the cause of sea ice loss. Typically, studies set newly ice-free SST to the freezing point of saltwater (e.g., Magnusdottir et al. 2004; Singarayer et al. 2006; Deser et al. 2010; Nakamura et al. 2015) or prescribe SSTs obtained from simulations of climate change (e.g., Screen et al. 2013; Peings and Magnusdottir 2014; Kim et al. 2014; Sun et al. 2015; Smith et al. 2019). If applied to our idealized model, each of these approaches would prescribe warmer SSTs than the newly ice-free SST obtained in our FRZ experiments, which is subfreezing at the ice edge by definition (because the freezing point has been reduced to induce sea ice loss). This implies that AGCM experiments may also include a spurious warming in polar regions, which will be exaggerated in cases where future SST is prescribed when sea ice is lost (notably including PAMIP; Smith et al. 2019).

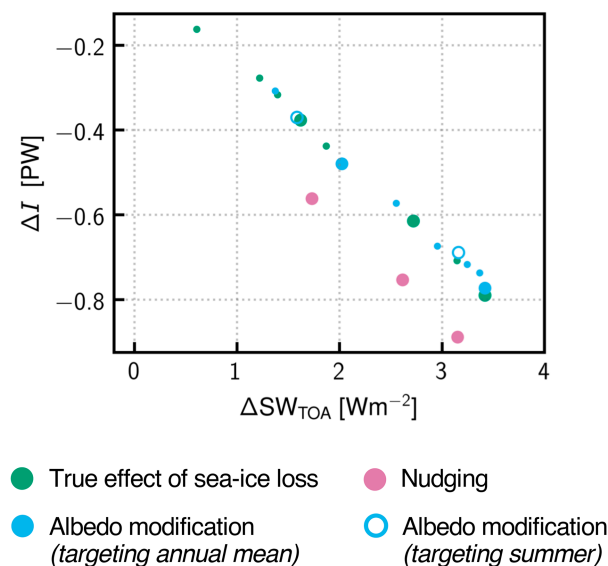
Storm track response vs. ΔSW_{TOA} 

FIG. 14. Response of storm-track intensity, I , to sea ice loss, as a function of the change in globally averaged net TOA shortwave radiation. As in Fig. 11, but for ice-constrained experiments that best match the target SIA obtained in the ODP1.05, ODP1.1, and ODP1.2 experiments that are plotted using a larger marker size.

Our results suggest that climate model simulations with constrained sea ice should be treated with caution. However, it is important to emphasize that across all of our idealized simulations, both with and without a spurious effect, the characteristics of the zonally averaged temperature and atmospheric circulation response to sea ice loss are largely the same, especially in DJF when the true response is greatest compared with other times of the year (Figs. 4 and 9). In each case, temperature increases at high latitudes in the lower troposphere, and the eddy-driven jet weakens on its poleward flank, accompanied by a reduction in storm-track activity. These results are broadly consistent with those obtained using sophisticated AGCMs (e.g., Smith et al. 2022) and AOGCMs (e.g., Screen et al. 2018). Spurious warming associated with ice-constraining methods serves mostly to increase the magnitude of the response, but it is not the only cause of uncertainty in this respect. For example, there is significant spread in the magnitude of the midlatitude jet response obtained with AGCMs, potentially due to variation in the strength of eddy feedbacks between models (Smith et al. 2022). In addition, Peings and Magnusdottir (2014) highlight that different representations of clouds and aerosols in models may have a significant impact on the magnitude of the stratospheric polar vortex response to sea ice loss. Other factors that contribute to model spread include differences in the background state (Smith et al. 2017) and internal variability, especially in the stratosphere (Peings et al. 2021; Sun et al. 2022; Smith et al. 2022; Liang et al. 2024). Additional uncertainty arises due to model biases in the representation of the Arctic surface climate, for example, the negative temperature bias over Arctic sea ice obtained in CMIP models (Davy and Outten 2020). To more precisely constrain the circulation response to Arctic sea ice loss, it is equally important that sources of intermodel variability, model bias, and the effects of spurious heating are better understood.

Finally, it is important to note that the term spurious is open to interpretation. Screen et al. (2013) argue that the emergence of newly ice-free areas with warmed SSTs is inseparable from sea ice loss and so should be included in simulations that investigate the climate response to sea ice loss. Within this context, it may be argued that the appropriateness (or otherwise) of current AGCM and AOGCM experiments depends on the framing of the science question under consideration. Specifically, existing experiments with constrained sea ice implicitly target the following question:

Q1. What is the difference between the current climate and a counterfactual climate where sea ice is artificially melted?

Our intention is not to suggest that studying this question is without merit but instead to stress that it is important to acknowledge the nuance that differentiates this question from the alternate question:

Q2. What is the effect of sea ice loss on climate?

Acknowledgments. We would like to acknowledge three anonymous reviewers whose feedback helped us improve this study throughout. Additionally, we thank Paul Kushner and Luke Fraser-Leach for engaging in discussion that benefited this

work. NTL, JAS, RG, WJMS, and SIT acknowledge support from the Natural Environment Research Council (NERC) under Grant Agreement ArctiCONNECT (NE/V005855/1). MRE is supported by an 1851 Research Fellowship. RM is funded by an NERC GW4+ Doctoral Training Partnership studentship (NE/S007504/1).

Data availability statement. The code required to run the Isca experiments used in this work is available at <https://github.com/ExeClim/Isca/pull/266>. Model output data are available at <https://zenodo.org/doi/10.5281/zenodo.11547752>.

APPENDIX

Storm-Track Response to Spurious Energy Input

To interpret the effect of spurious energy input on the storm-track intensity response ΔI , we make use of the MSE framework described by Shaw et al. (2018) and Shaw and Smith (2022). The meridional MSE budget is given by

$$\nabla \cdot F_{TE} = Ra + TF - \nabla \cdot F_M, \quad (A1)$$

where Ra is radiative cooling (the difference between net downward top of atmosphere and surface radiative fluxes), TF is the surface turbulent flux into the atmosphere, and $F_M = \overline{v\bar{m}}$ is the meridional MSE flux due to the mean circulation. Above, Ra and TF have their global-mean removed, following Kang et al. (2008) and Shaw and Smith (2022). By making use of the surface energy budget,

$$TF = SW_s + LW_s - \nabla \cdot F_{NA}, \quad (A2)$$

Equation (A1) can be rewritten as

$$\nabla \cdot F_{TE} = SW_{TOA} + LW_{TOA} - \nabla \cdot F_M - \nabla \cdot F_{NA}, \quad (A3)$$

where SW_{TOA} and LW_{TOA} are the net downward top of atmosphere shortwave and longwave radiative fluxes and $\nabla \cdot F_{NA}$ denotes the energy flux divergence due to nonatmospheric processes, such as ocean heat transport and, in the case of the NDG experiments, artificial energy input used to remove sea ice.

Using Eq. (A3), a change in storm-track intensity between climates can be written as

$$\Delta I = \Delta I_{SW} + \Delta I_{LW} - \Delta I_M - \Delta I_{NA}, \quad (A4)$$

by meridionally integrating Eq. (A3) from the pole to a latitude ϑ (ΔI_{SW} and ΔI_{LW} have their global mean removed; Kang et al. 2008; Shaw and Smith 2022). For our purposes, we take the two climates of interest to be those obtained in a FRZ experiment (the true effect of sea ice loss) and the corresponding nudging or albedo modification experiment.

The spurious response of nonatmospheric energy transport is due to nudging, as in our idealized model, ocean heat transport does not change between experiments. Likewise, the spurious response of top of atmosphere shortwave is determined solely

by the upward shortwave flux, as the downward flux does not change between in experiments. Furthermore, in the idealized model, only changes in the surface albedo can affect the upward shortwave flux, which is the same at the surface and the top of atmosphere. The FRZ experiments capture the true response of surface albedo to sea ice loss, so any differences between the albedo in NDG or ALB experiments and FRZ experiments are spurious. Taken together, these observations allow us to rewrite Eq. (A4) as an equation for the spurious response of the storm-track intensity, ΔI^* , to spurious energy input associated with the nudging and albedo modification methodologies:

$$\Delta I^* = \Delta I_{LW}^* - \Delta I_M^* + \Delta I_{input}^*, \quad (\text{A5})$$

with

$$\Delta I_{input}^* = 2\pi a^2 \int_{\pi/2}^{\theta} (F_{nudge} - \Delta\alpha_{sfc} F_{sw,sfc}^{\downarrow}) \cos\theta d\theta, \quad (\text{A6})$$

which are Eqs. (20) and (21) in the main text, respectively. Here, the asterisks denote a spurious forcing or response, and all differences are computed between experiments with spurious additional heating to melt ice (i.e., NDG and ALB) and the FRZ experiments, which do not introduce additional heating.

REFERENCES

- Ayres, H. C., J. A. Screen, E. W. Blockley, and T. J. Bracegirdle, 2022: The coupled atmosphere–ocean response to Antarctic sea ice loss. *J. Climate*, **35**, 4665–4685, <https://doi.org/10.1175/JCLI-D-21-0918.1>.
- Barnes, E. A., and J. A. Screen, 2015: The impact of Arctic warming on the midlatitude jet-stream: Can it? Has it? Will it? *Wiley Interdiscip. Rev.: Climate Change*, **6**, 277–286, <https://doi.org/10.1002/wcc.337>.
- Blackport, R., and P. J. Kushner, 2016: The transient and equilibrium climate response to rapid summertime sea ice loss in CCSM4. *J. Climate*, **29**, 401–417, <https://doi.org/10.1175/JCLI-D-15-0284.1>.
- , and —, 2017: Isolating the atmospheric circulation response to Arctic sea ice loss in the coupled climate system. *J. Climate*, **30**, 2163–2185, <https://doi.org/10.1175/JCLI-D-16-0257.1>.
- , and —, 2018: The role of extratropical ocean warming in the coupled climate response to Arctic sea ice loss. *J. Climate*, **31**, 9193–9206, <https://doi.org/10.1175/JCLI-D-18-0192.1>.
- Bordoni, S., 2007: On the role of eddies in monsoonal circulations: Observations and theory. Ph.D. thesis, University of California, 195 pp.
- Chen, L., R. Wu, Q. Shu, C. Min, Q. Yang, and B. Han, 2023: The Arctic sea ice thickness change in CMIP6's historical simulations. *Adv. Atmos. Sci.*, **40**, 2331–2343, <https://doi.org/10.1007/s00376-022-1460-4>.
- Chung, E.-S., K.-J. Ha, A. Timmermann, M. F. Stuecker, T. Bodai, and S.-K. Lee, 2021: Cold-season Arctic amplification driven by Arctic Ocean mediated seasonal energy transfer. *Earth's Future*, **9**, e2020EF001898, <https://doi.org/10.1029/2020EF001898>.
- Chung, P.-C., and N. Feldl, 2024: Sea ice loss, water vapor increases, and their interactions with atmospheric energy transport in driving seasonal polar amplification. *J. Climate*, **37**, 2713–2725, <https://doi.org/10.31223/X5768P>.
- Cohen, J., and Coauthors, 2014: Recent Arctic amplification and extreme mid-latitude weather. *Nat. Geosci.*, **7**, 627–637, <https://doi.org/10.1038/ngeo2234>.
- , and Coauthors, 2020: Divergent consensus on Arctic amplification influence on midlatitude severe winter weather. *Nat. Climate Change*, **10**, 20–29, <https://doi.org/10.1038/s41558-019-0662-y>.
- Davis, N. A., and T. Birner, 2022: Eddy-mediated Hadley cell expansion due to axisymmetric angular momentum adjustment to greenhouse gas forcings. *J. Atmos. Sci.*, **79**, 141–159, <https://doi.org/10.1175/JAS-D-20-0149.1>.
- Davy, R., and S. Outten, 2020: The Arctic surface climate in CMIP6: Status and developments since CMIP5. *J. Climate*, **33**, 8047–8068, <https://doi.org/10.1175/JCLI-D-19-0990.1>.
- Deser, C., R. Tomas, M. Alexander, and D. Lawrence, 2010: The seasonal atmospheric response to projected Arctic sea ice loss in the late twenty-first century. *J. Climate*, **23**, 333–351, <https://doi.org/10.1175/2009JCLI3053.1>.
- , R. A. Tomas, and L. Sun, 2015: The role of ocean–atmosphere coupling in the zonal-mean atmospheric response to Arctic sea ice loss. *J. Climate*, **28**, 2168–2186, <https://doi.org/10.1175/JCLI-D-14-00325.1>.
- England, M. R., and N. Feldl, 2024: Robust polar amplification in ice-free climates relies on ocean heat transport and cloud radiative effects. *J. Climate*, **37**, 2179–2197, <https://doi.org/10.1175/JCLI-D-23-0151.1>.
- , L. M. Polvani, L. Sun, and C. Deser, 2020: Tropical climate responses to projected Arctic and Antarctic sea-ice loss. *Nat. Geosci.*, **13**, 275–281, <https://doi.org/10.1038/s41561-020-0546-9>.
- , I. Eisenman, and T. J. W. Wagner, 2022: Spurious climate impacts in coupled sea ice loss simulations. *J. Climate*, **35**, 7401–7411, <https://doi.org/10.1175/JCLI-D-21-0647.1>.
- Feldl, N., and T. M. Merlis, 2021: Polar amplification in idealized climates: The role of ice, moisture, and seasons. *Geophys. Res. Lett.*, **48**, e2021GL094130, <https://doi.org/10.1029/2021GL094130>.
- Fraser-Leach, L., P. Kushner, and A. Audette, 2024: Correcting for artificial heat in coupled sea ice perturbation experiments. *Environ. Res. Climate*, **3**, 015003, <https://doi.org/10.1088/2752-5295/ad1334>.
- Frierson, D. M. W., 2007: The dynamics of idealized convection schemes and their effect on the zonally averaged tropical circulation. *J. Atmos. Sci.*, **64**, 1959–1976, <https://doi.org/10.1175/JAS3935.1>.
- , I. M. Held, and P. Zurita-Gotor, 2006: A gray-radiation aquaplanet moist GCM. Part I: Static stability and eddy scale. *J. Atmos. Sci.*, **63**, 2548–2566, <https://doi.org/10.1175/JAS3753.1>.
- Hahn, L. C., K. C. Armour, M. D. Zelinka, C. M. Bitz, and A. Donohoe, 2021: Contributions to polar amplification in CMIP5 and CMIP6 models. *Front. Earth Sci.*, **9**, 710036, <https://doi.org/10.3389/feart.2021.710036>.
- , —, D. S. Battisti, I. Eisenman, and C. M. Bitz, 2022: Seasonality in Arctic warming driven by sea ice effective heat capacity. *J. Climate*, **35**, 1629–1642, <https://doi.org/10.1175/JCLI-D-21-0626.1>.
- Hwang, Y.-T., D. M. W. Frierson, and J. E. Kay, 2011: Coupling between Arctic feedbacks and changes in poleward energy transport. *Geophys. Res. Lett.*, **38**, L17704, <https://doi.org/10.1029/2011GL048546>.
- Kang, S. M., I. M. Held, D. M. W. Frierson, and M. Zhao, 2008: The response of the ITCZ to extratropical thermal forcing:

- Idealized slab-ocean experiments with a GCM. *J. Climate*, **21**, 3521–3532, <https://doi.org/10.1175/2007JCLI2146.1>.
- Kim, B.-M., S.-W. Son, S.-K. Min, J.-H. Jeong, S.-J. Kim, X. Zhang, T. Shim, and J.-H. Yoon, 2014: Weakening of the stratospheric polar vortex by Arctic sea-ice loss. *Nat. Commun.*, **5**, 4646, <https://doi.org/10.1038/ncomms5646>.
- Kwok, R., 2018: Arctic sea ice thickness, volume, and multiyear ice coverage: Losses and coupled variability (1958–2018). *Environ. Res. Lett.*, **13**, 105005, <https://doi.org/10.1088/1748-9326/aae3ec>.
- Lewis, N. T., W. J. M. Seviour, H. E. Roberts-Straw, and J. A. Screen, 2024: The response of surface temperature persistence to Arctic sea-ice loss. *Geophys. Res. Lett.*, **51**, e2023GL106863, <https://doi.org/10.1029/2023GL106863>.
- Liang, Y.-C., L. M. Polvani, and I. Mitevski, 2022: Arctic amplification, and its seasonal migration, over a wide range of abrupt CO₂ forcing. *npj Climate Atmos. Sci.*, **5**, 14, <https://doi.org/10.1038/s41612-022-00228-8>.
- , and Coauthors, 2024: The weakening of the stratospheric polar vortex and the subsequent surface impacts as consequences to Arctic sea ice loss. *J. Climate*, **37**, 309–333, <https://doi.org/10.1175/JCLI-D-23-0128.1>.
- Lu, J., and M. Cai, 2009: Seasonality of polar surface warming amplification in climate simulations. *Geophys. Res. Lett.*, **36**, L16704, <https://doi.org/10.1029/2009GL040133>.
- Magnusdottir, G., C. Deser, and R. Saravanan, 2004: The effects of North Atlantic SST and sea ice anomalies on the winter circulation in CCM3. Part I: Main features and storm track characteristics of the response. *J. Climate*, **17**, 857–876, [https://doi.org/10.1175/1520-0442\(2004\)017<0857:TEONAS>2.0.CO;2](https://doi.org/10.1175/1520-0442(2004)017<0857:TEONAS>2.0.CO;2).
- McCusker, K. E., P. J. Kushner, J. C. Fyfe, M. Sigmond, V. V. Kharin, and C. M. Bitz, 2017: Remarkable separability of circulation response to Arctic sea ice loss and greenhouse gas forcing. *Geophys. Res. Lett.*, **44**, 7955–7964, <https://doi.org/10.1002/2017GL074327>.
- Merlis, T. M., and M. Henry, 2018: Simple estimates of polar amplification in moist diffusive energy balance models. *J. Climate*, **31**, 5811–5824, <https://doi.org/10.1175/JCLI-D-17-0578.1>.
- , T. Schneider, S. Bordoni, and I. Eisenman, 2013: Hadley circulation response to orbital precession. Part II: Subtropical continent. *J. Climate*, **26**, 754–771, <https://doi.org/10.1175/JCLI-D-12-00149.1>.
- Nakamura, T., K. Yamazaki, K. Iwamoto, M. Honda, Y. Miyoshi, Y. Ogawa, and J. Ukita, 2015: A negative phase shift of the winter AO/NAO due to the recent Arctic sea-ice reduction in late autumn. *J. Geophys. Res. Atmos.*, **120**, 3209–3227, <https://doi.org/10.1002/2014JD022848>.
- Notz, D., and J. Stroeve, 2016: Observed Arctic sea-ice loss directly follows anthropogenic CO₂ emission. *Science*, **354**, 747–750, <https://doi.org/10.1126/science.aag2345>.
- O’Gorman, P. A., and T. Schneider, 2008: The hydrological cycle over a wide range of climates simulated with an idealized GCM. *J. Climate*, **21**, 3815–3832, <https://doi.org/10.1175/2007JCLI2065.1>.
- Peings, Y., and G. Magnusdottir, 2014: Response of the winter-time Northern Hemisphere atmospheric circulation to current and projected Arctic sea ice decline: A numerical study with CAM5. *J. Climate*, **27**, 244–264, <https://doi.org/10.1175/JCLI-D-13-00272.1>.
- , Z. M. Labe, and G. Magnusdottir, 2021: Are 100 ensemble members enough to capture the remote atmospheric response to +2°C Arctic sea ice loss? *J. Climate*, **34**, 3751–3769, <https://doi.org/10.1175/JCLI-D-20-0613.1>.
- Schweiger, A., R. Lindsay, J. Zhang, M. Steele, H. Stern, and R. Kwok, 2011: Uncertainty in modeled Arctic sea ice volume. *J. Geophys. Res.*, **116**, C00D06, <https://doi.org/10.1029/2011JC007084>.
- Screen, J. A., and I. Simmonds, 2010a: Increasing fall-winter energy loss from the Arctic Ocean and its role in Arctic temperature amplification. *Geophys. Res. Lett.*, **37**, L16707, <https://doi.org/10.1029/2010GL044136>.
- , and —, 2010b: The central role of diminishing sea ice in recent Arctic temperature amplification. *Nature*, **464**, 1334–1337, <https://doi.org/10.1038/nature09051>.
- , —, C. Deser, and R. Tomas, 2013: The atmospheric response to three decades of observed Arctic sea ice loss. *J. Climate*, **26**, 1230–1248, <https://doi.org/10.1175/JCLI-D-12-00063.1>.
- , and Coauthors, 2018: Consistency and discrepancy in the atmospheric response to Arctic sea-ice loss across climate models. *Nat. Geosci.*, **11**, 155–163, <https://doi.org/10.1038/s41561-018-0059-y>.
- Semtner, A. J., Jr., 1976: A model for the thermodynamic growth of sea ice in numerical investigations of climate. *J. Phys. Oceanogr.*, **6**, 379–389, [https://doi.org/10.1175/1520-0485\(1976\)006<0379:AMFTTG>2.0.CO;2](https://doi.org/10.1175/1520-0485(1976)006<0379:AMFTTG>2.0.CO;2).
- Shaw, T. A., and Z. Smith, 2022: The midlatitude response to polar sea ice loss: Idealized slab-ocean aquaplanet experiments with thermodynamic sea ice. *J. Climate*, **35**, 2633–2649, <https://doi.org/10.1175/JCLI-D-21-0508.1>.
- , P. Barpanda, and A. Donohoe, 2018: A moist static energy framework for zonal-mean storm-track intensity. *J. Atmos. Sci.*, **75**, 1979–1994, <https://doi.org/10.1175/JAS-D-17-0183.1>.
- Singarayer, J. S., J. L. Bamber, and P. J. Valdes, 2006: Twenty-first-century climate impacts from a declining Arctic sea ice cover. *J. Climate*, **19**, 1109–1125, <https://doi.org/10.1175/JCLI3649.1>.
- Smith, D. M., N. J. Dunstone, A. A. Scaife, E. K. Fiedler, D. Copsey, and S. C. Hardiman, 2017: Atmospheric response to Arctic and Antarctic sea ice: The importance of ocean–atmosphere coupling and the background state. *J. Climate*, **30**, 4547–4565, <https://doi.org/10.1175/JCLI-D-16-0564.1>.
- , and Coauthors, 2019: The Polar Amplification Model Inter-comparison Project (PAMIP) contribution to CMIP6: Investigating the causes and consequences of polar amplification. *Geosci. Model Dev.*, **12**, 1139–1164, <https://doi.org/10.5194/gmd-12-1139-2019>.
- , and Coauthors, 2022: Robust but weak winter atmospheric circulation response to future Arctic sea ice loss. *Nat. Commun.*, **13**, 727, <https://doi.org/10.1038/s41467-022-28283-y>.
- Sun, L., C. Deser, and R. A. Tomas, 2015: Mechanisms of stratospheric and tropospheric circulation response to projected Arctic sea ice loss. *J. Climate*, **28**, 7824–7845, <https://doi.org/10.1175/JCLI-D-15-0169.1>.
- , —, —, and M. Alexander, 2020: Global coupled climate response to polar sea ice loss: Evaluating the effectiveness of different ice-constraining approaches. *Geophys. Res. Lett.*, **47**, e2019GL085788, <https://doi.org/10.1029/2019GL085788>.
- , —, I. Simpson, and M. Sigmond, 2022: Uncertainty in the winter tropospheric response to Arctic sea ice loss: The role of stratospheric polar vortex internal variability. *J. Climate*, **35**, 3109–3130, <https://doi.org/10.1175/JCLI-D-21-0543.1>.
- Tan, Z., O. Lachmy, and T. A. Shaw, 2019: The sensitivity of the jet stream response to climate change to radiative assumptions. *J. Adv. Model. Earth Syst.*, **11**, 934–956, <https://doi.org/10.1029/2018MS001492>.

- Tomas, R. A., C. Deser, and L. Sun, 2016: The role of ocean heat transport in the global climate response to projected Arctic sea ice loss. *J. Climate*, **29**, 6841–6859, <https://doi.org/10.1175/JCLI-D-15-0651.1>.
- Troen, I. B., and L. Mahrt, 1986: A simple model of the atmospheric boundary layer; sensitivity to surface evaporation. *Bound.-Layer Meteor.*, **37**, 129–148, <https://doi.org/10.1007/BF00122760>.
- Vallis, G. K., 2017: *Atmospheric and Oceanic Fluid Dynamics: Fundamentals and Large-Scale Circulation*. Cambridge University Press, 946 pp., <https://doi.org/10.1017/9781107588417>.
- , and Coauthors, 2018: Isca, v1.0: A framework for the global modelling of the atmospheres of Earth and other planets at varying levels of complexity. *Geosci. Model Dev.*, **11**, 843–859, <https://doi.org/10.5194/gmd-11-843-2018>.
- Wang, K., C. Deser, L. Sun, and R. A. Tomas, 2018: Fast response of the tropics to an abrupt loss of Arctic sea ice via ocean dynamics. *Geophys. Res. Lett.*, **45**, 4264–4272, <https://doi.org/10.1029/2018GL077325>.
- Winkelbauer, S., M. Mayer, and L. Haimberger, 2024: Validation of key Arctic energy and water budget components in CMIP6. *Climate Dyn.*, **62**, 3891–3926, <https://doi.org/10.1007/s00382-024-07105-5>.
- Zhang, X., T. Schneider, Z. Shen, K. G. Pressel, and I. Eisenman, 2022: Seasonal cycle of idealized polar clouds: Large eddy simulations driven by a GCM. *J. Adv. Model. Earth Syst.*, **14**, e2021MS002671, <https://doi.org/10.1029/2021MS002671>.